Microbiota-derived secondary bile acids promote STING activation and antitumor activity

Authors: Xinglin Yang[1,4*†], Xing Zhang[1†], Weichao Li[2], Anant Gharpure[3], Althea Hansel-Harris[3], Andreas F. Tillack[3], Chongyang Wu[1], Yan-Zhu Hsieh[1], Ariana Sulpizio[2], Kyong T. Fam[1], Stanislav Dikiy[1], Xiaohui Zhao[1], Stefano Forli[3], Luke L. Lairson[2], Andrew Ward[3], Christopher G. Parker[2], Howard C. Hang[1,2*]

Affiliations:

[1] Department of Immunology and Microbiology, Scripps Research

[2] Department of Chemistry, Scripps Research

[3] Department of Integrative Structural and Computational Biology, Scripps Research

[4] State Key Laboratory of Natural and Biomimetic Drugs, School of Pharmaceutical Sciences, Chemical Biology Center, Peking University

[†]These authors contributed equally to this work

*Corresponding authors. xlyang@hsc.pku.edu.cn (X. Y.); hhang@scripps.edu (H. C. H.).

Abstract: Microbiota metabolism generates diverse bile acids that are associated with health and disease, but the molecular targets and mechanisms of action for these metabolites have not been fully elucidated. Using bile acid photoaffinity probes and chemoproteomics, we found many protein targets of microbiota-derived secondary bile acids in mammalian cells. Of note, we discovered deoxycholic acid (DCA) binds the transmembrane domain of stimulator of interferon genes (STING), promotes its oligomerization and agonist stimulation of type I interferon signaling *ex vivo* and antitumor immunity *in vivo*. Moreover, oral administration of DCA-producing microbiota species enhanced STING agonist antitumor immunity *in vivo*. This reverse chemical microbiology approach revealed an unpredicted mechanism of action for DCA on STING regulation and suggests specific secondary bile acids and their associated microbiota species may impact the efficacy of STING-targeted therapeutics.

Main Text:

Bile acids are sterol metabolites that are associated with diverse phenotypes in health, disease and therapy responses(*1*), but their specific mechanisms of action are still enigmatic. Biosynthesis of bile acids starts with oxidation and hydroxylation of cholesterol in the liver followed by conjugation with glycine or taurine to generate primary bile acids(*1*). Export of primary bile acids into the intestine facilitates cholesterol turnover and disposal as well as aids in digestion. In the gut, primary bile acids are deconjugated, oxidized and epimerized by specific microbiota species to generate a variety of secondary bile acids(*2-5*) (**Fig. 1a**). In recent years, these structurally diverse microbiota-derived bile acids have emerged as signaling molecules that regulate variety physiological processes, ranging from direct antibacterial activity(*6, 7*) to modulation of host metabolism(*8-11*), immunity(*12, 13*), viral infection(*14, 15*), vaccine responses(*16*), aging(*7, 17*) and tumor progression (*18-22*). Of note, bile acids were discovered as endogenous ligands for farnesoid X receptor (FXR), which regulates the expression of target genes involved in hepatic bile acid synthesis, secretion and intestinal re-absorption(*23, 24*) and are also implicated in T cell-driven inflammation(*13*). In addition, the G-protein coupled receptor TGR5 has been reported to sense bile acids and regulate intestinal homeostasis and inflammation(*12, 25*). Moreover, secondary bile acids have been reported to bind and regulate the activity of specific nuclear hormone receptors like RORγt and NR4A1 in T cells to control their differentiation and activation(*26-30*). Secondary bile acids have also been shown to phenocopy anti-aging effects of calorie restriction by binding TUB-like protein□3(*17, 31*). Metabolomic studies indicate hundreds of additional conjugated and unconjugated bile acids can be found in different mammalian tissues(*4, 9*), which necessitates further mechanistic and functional studies.

DCA directly binds to STING

To address the mechanisms of actions for different bile acids, we and others have generated photoaffinity probes to identify and validate their protein targets in bacteria(*32-35*) and mammalian cells(*31, 36*) (**Extended Data Fig. 1a**). In this study, we focused on deoxycholic acid (DCA) (**Fig. 1a**), as this microbiota-derived secondary bile acid has been reported to modulate host immunity(*14, 16*) and also been developed a therapeutic to reduce submental fat(*37*), but the protein targets of DCA and its mechanisms of action have not been fully elucidated. DCA is a secondary bile acid generated by the gut microbiota dehydroxylation of cholic acid (CA) (**Fig. 1a**). The removal of a hydroxyl group at the C7 of the sterol significantly alters the physicochemical properties of the bile acid, potentially conferring unique membrane penetrating and protein binding capabilities of DCA. Using different photoaffinity probes for DCA and CA (**Fig. 1b, Extended Data Fig. 1a**), our quantitative comparative chemoproteomic analysis of human monocyte (THP-1) cell line revealed many candidate DCA-selective protein targets (**Fig. 1c, d**), including sterol metabolic enzymes, membrane proteins, nuclear receptors and immunity-associated proteins (**Extended Data Fig. 1b, Tables S1-3, supplementary Data S1**). Notably, STING (TMEM173) was one of the DCA-selective protein targets compared to CA and can be competed off by excess of DCA (**Fig. 1c, d, Extended Data Fig. 1b**). Western blot analysis of photoaffinity probe-enriched proteins showed that STING was crosslinked by the DCA probes, but not the CA probe, which was significantly reduced when THP-1 cells were co-incubated DCA (**Fig. 1e**). DCA also reduced photoaffinity probe crosslinking of FXR and STING endogenously expressed in HT-29 cells (**Extended Data Fig. 1c**) and human STING overexpressed in HEK293T cells (**Extended Data Fig. 1d**). These results suggest that DCA may directly bind STING in mammalian cells.

STING is a critical immune sensor activated by cyclic dinucleotides (CDNs), which can be synthesized by cyclic GMP-AMP synthase (cGAS) in response to endogenous cytosolic DNA fragments or from pathogens during infection(*38, 39*). Upon binding CDNs, STING that localized to the endoplasmic reticulum (ER), oligomerizes, translocates to endolysosomes and forms a complex with TANK-binding kinase 1 (TBK1). TBK1 then phosphorylates itself, STING and transcription factors such as interferon regulatory factor 3 (IRF3), which activates IRF3 to induce the production of type I interferons (IFNs) and other cytokines to promote immune responses against infections and tumors(*40, 41*). In addition, TBK1 recruitment to STING also activates NF-κB signaling.(*42*) Based on these properties, synthetic agonists for STING have been developed as therapeutic leads to treat infections(*29, 43*) and cancer(*44, 45*). Of note, compounds that mimic CDNs such as diABZI(*46*), SR-717(*47*) and MSA-2(*48*) (**Extended Data Fig. 2a**) have been shown to target the CDN-binding domain of STING and potently induce the expression of type I IFN responses. Furthermore, compounds such as C53(*49*) and NVS-STG2(*50*) that bind the transmembrane domain of STING also promote its oligomerization and immune activation (**Extended Data Fig. 2b**). Chemoproteomic and *in vitro* studies have also suggested cholesterol may bind the CRAC motif of STING and facilitate retention of STING oligomers in the endoplasmic reticulum, which revealed STING activation may be tuned by alterations in cholesterol homeostasis(*51, 52*). However, whether bile acids such as DCA can directly bind and impact STING activation was unknown.

Bile acids promote STING activation *ex vivo*

We therefore investigated if DCA alone or in combination with STING agonists modulated type I IFN responses. Using an IFN-β luciferase reporter assay, we found that DCA but not CA

enhanced the activity of CDNs (cGAMP and c-di-AMP) and synthetic STING agonists such as diABZI (**Fig. 2a, Extended Data Fig. 2e**). DCA alone did not significantly activate STING at concentrations up to 200 μM, but enhanced the activity of diABZI in a dose-dependent manner by measuring STING phosphorylation in THP-1 cells (**Extended Data Fig. 2c, d**). To further investigate the STING activation, we measured the expression of IFN-β, CXCL10, and IL-6 in both THP-1 and RAW264.7 (murine macrophage cell line) using RT-qPCR (**Fig. 2b**). Co-treatment with DCA and diABZI induced significantly higher levels of these cytokines compared to either treatment alone (**Fig. 2b**). Treatment of THP-1 cells with DCA and diABZI increased the phosphorylation of STING, TBK1, and IRF3 compared to either compound alone, which was also abrogated in STING knockout (KO) cells (**Fig. 2c**).

To further characterize the scope and specificity of DCA-STING activation, we transfected differentiated THP-1 cells with high molecular weight DNA (HT-DNA), which activates cGAS to produce endogenous cGAMP and observed DCA enhancement of HT-DNA induced STING activation (**Extended Data Fig. 3a**). DCA also enhanced the activity of other synthetic STING agonists (SR-717, MSA-2 and DMXAA) in HEK293T cells expressing human STING and an IFN-β reporter (**Extended Data Fig. 3b**) as well as other STING variants, including murine STING, STING-HAQ (R71H, G230A and R293Q), and STING-232H (R232H)(*53*) (**Extended Data Fig. 3c**). DCA enhancement of STING activation was also observed with CDNs (**Fig. 2d,e**) and diABZI in primary human peripheral blood mononuclear cells (PBMCs) (**Fig. 2f,g, Extended Data Fig. 2f**) as well as differentiated THP-1 (**Extended Data Fig. 3d**) and HT-29 cells (**Extended Data Fig. 3e**). We also observed more STING puncta formation (**Extended Data Fig. 4a,b**) and oligomerization (**Extended Data Fig. 4c**) in cells that were co-treated with diABZI and DCA, but not CA. Interestingly, pre-treatment of THP-1 cells with diABZI

enhanced the interaction between the DCA probe and STING (**Extended Data Fig. 4d,e**). This enhanced interaction was suppressed by BB-Cl (**Extended Data Fig. 4d,e**), an inhibitor of STING activation (**Extended Data Fig. 4f**)(*54*).

Bile acids bind STING dimer-dimer interface

To investigate the binding site of DCA on STING, we conducted competitive ligand photoaffinity crosslinking studies in cells and structural studies *in vitro*. Notably, NVS-STG2 a synthetic molecule reported to target the STING dimer-dimer interface reduced DCA probe photocrosslinking with STING in cells (**Fig. 3a,b**). In contrast, diABZI which binds the CDN-binding domain failed to affect the DCA probe-STING photocrosslinking, even with 10-fold excess (**Extended Data Fig. 4g**). To elucidate the DCA-STING binding site, we employed single-particle cryo-electron microscopy (cryo-EM). We included STING agonists cGAMP and C53 to capture the ligand-activated protein state and stabilize potential oligomers, similar to previous studies with NVS-STG2(*55*). From these studies, we obtained a 2.9 Å resolution map of a STING tetramer complexed with ligands (cGAMP, C53 and DCA) (**Extended Data Fig. 5**). Notably, we observed additional molecular density between the transmembrane domains of STING dimers (**Fig. 3c**), which was absent in the STING-cGAMP-C53 structure(*49*), suggesting this region as a potential binding site for secondary bile acids like DCA. To determine DCA occupancy of the STING dimer interface, we used a custom Monte-Carlo docking engine. Affinity grid maps were calculated with the AutoDock4.2 force field and modified using our CryoXKit(*56*) software to include guidance from the C2-symmetric cryo-EM density. The resulting docked model is shown in **Extended Data Fig. 6a**, where we have modeled one bile acid molecule into one half of the C2 map. The carboxylate of DCA forms strong charge-charge

interactions with R94 of both the A (red) and C (blue) STING monomers, vertically orienting the ligand parallel to the surrounding helices. The rest of the molecule forms interactions mostly with the A and B (yellow) monomers. This single, static binding pose only explains a limited portion of the observed ligand density. Therefore, we generated a Boltzmann-weighted map of all poses sampled during the docking simulation, to better represent the full volume sampled during the run and allow for more direct comparison to the cryoEM density. Notably, this map also includes the sampled positions of oxygens and polar hydrogens that may be poorly resolved in the corresponding cryoEM density. The docking Boltzmann map (outer purple surface in **Extended Data Fig. 6b**) shows that the docking does largely sample all the cryoEM density volumes assigned to the ligand, including those not explained by the single predicted binding pose. These results suggest that DCA may bind at the STING transmembrane dimer-dimer interface to enhance oligomerization and promote agonist-induced activation.

To validate the proposed bile acid binding site, we generated STING transmembrane mutants and assessed their response to diABZI and DCA. Several mutants, such as L136A, L136K, and L136R, showed increased sensitivity to DCA activation in HEK293T cells (**Fig. 3d**). In contrast, other STING mutants, including R94F, R95F, and L136E, exhibited reduced sensitivity to DCA-induced enhancement of STING activation in HEK293T cells (**Fig. 3d**). Expression of these STING mutants in HEK293T (**Fig. 3e-f**) or STING-KO THP-1 cells (**Extended Data Fig. 6c**), which are reported to express other bile acid receptors such FXR(*57*) and TGR5(*15*), still showed attenuated DCA enhancement of diABZI-induced STING activation (**Extended Data Fig. 6c**). These mutagenesis and activity data support the model that DCA binds directly to the STING transmembrane domain dimer-dimer interface to modulate immune signaling.

To assess the specificity of BAs on STING activation, we compared the effects of different conjugated and free bile acids. DCA consistently exhibited the most potent activity among all tested BAs (**Extended Data Fig. 6d**). Structural modifications at the 3-hydroxyl position, such as isomerization or oxidation, significantly reduced DCA enhancement of STING activation (**Extended Data Fig. 6d**). Interestingly, alloLCA, but not LCA or isoLCA, showed comparable levels of DCA enhanced STING activation (**Extended Data Fig. 6d**). These results demonstrate DCA, amongst the BAs tested, most effectively enhances STING activation in a variety of different cell types *ex vivo*. Molecular docking of other bile acids (**Extended Data Fig. 6e**) shows the inactive sterols (CA, iso-DCA, UDCA and iso-LCA) do not make ideal contacts with STING transmembrane dimer-dimer interface compared to other active secondary bile acids such as alloLCA (**Extended Data Fig. 6d**), which adopts similar conformation to DCA (**Extended Data Fig. 6a**). Together, these findings indicate that secondary bile acids such as DCA binds to a large pocket at the STING transmembrane dimer-dimer interface to enhance its ligand-induced oligomerization and activation of downstream signaling.

DCA boost STING agonist antitumor immunity

As STING activation has been shown to promote antitumor immunity(*44*, *45*), we evaluated the bile acids with diABZI in tumor models. For these studies, we employed intratumoral (IT) injection of the compounds (**Fig. 4a**) in the subcutaneous tumor models (*58*) and utilized a lower dose of diABZI (**Extended Data Fig. 7a**) to observe potential synergistic effects of the bile acids. IT injection of DCA (2.5 mg/kg) combined with a low dose of diABZI (50 μg/kg) significantly reduced tumor size, whereas neither treatment alone showed an effect (**Fig. 4b,**

Extended Data Fig. 7b). Notably, this effect was DCA-specific, as CA together with diABZI showed no antitumor activity against B16F10 melanoma tumors (**Fig. 4c**). We also found that DCA promoted diABZI-induced STING antitumor activity with less immunogenic Panc02 pancreatic tumors(*59*) (**Extended Data Fig. 7c**), whereas DCA did not have a significant effect on highly immunogenic MC38 colonic tumors (**Extended Data Fig. 7d**). To investigate the antitumor immune response, we analyzed the tumor-infiltrating lymphocytes (TILs), tumor-draining lymph nodes (tdLN) and spleen from B16F10-bearing mice by flow cytometry (**Supplementary Fig. 1**). diABZI treatment, with or without DCA, significantly upregulated Sca-1 across all three tissues, while the combination of DCA and diABZI selectively enhanced Sca-1 expression in tumors (**Fig. 4d, Extended Data Fig. 8a, b**). This increase occurred without changes in the absolute number of $CD45^+$ leukocytes or $CD3^+$ lymphocytes in TILs (**Extended Data Fig. 8c, d**). However, CD8□ T cells from the combination treatment group displayed significantly higher levels of activation markers, including CD69 (**Fig. 4e**), granzyme B (**Fig. 4f**), Ki-67 (**Fig. 4g**), and PD-1(**Fig. 4h**). In addition, both the frequency and granzyme B expression of NK1.1□ cells were elevated in the DCA + diABZI group (**Extended Data Fig. 8e, f**). These results show DCA enhancement of STING activation in TILs is sufficient to promote antitumor immunity *in vivo*.

Microbiota-producing DCA promote STING activation

Our discovery that DCA modulates STING activation suggests that specific microbiota species capable of producing secondary bile acids may regulate this immune signaling pathway *in vivo*. Of note, specific microbiota species such as *Akkermansia muciniphila* have been reported to secrete cyclic dinucleotides (CDNs) that directly activate the STING pathway and regulate

intratumoral IFN-I signaling(*60*). Other microbiota species have also been shown to enhance the efficacy of immune checkpoint blockade (ICB) via STING activation by unknown mechanisms of action(*61-63*). However, whether microbiota-derived secondary bile acids such as DCA can boost the therapeutic efficacy of STING agonists was unknown. To address this, we evaluated STING-mediated IFN-β induction following intraperitoneal injection of diABZI in mice treated with or without the antibiotic cocktail (**Fig. 5a**). In specific-pathogen-free (SPF) mice, diABZI induced robust IFN-β expression, whereas antibiotic-treated mice showed markedly decreased IFN-β levels in serum (**Fig. 5b**) and cecum (**Fig. 5c**). To test whether bile acids can rescue STING activation in antibiotic-treated mice, we co-injected diABZI with bile acids into the Abx-treated mouse (**Extended Data Fig. 9a**) and found that DCA, but not CA, synergizes with diABZI to increase serum IFN-β (**Fig. 5d**) and IL-6 (**Fig. 5e**) levels. In addition, DCA synergized with CDN STING agonists such as c-di-AMP and enhance serum levels of IFN-β (**Extended Data Fig. 9b**). We also examined the effect of vancomycin (**Extended Data Fig. 9c**), an antibiotic that targets Gram-positive bacteria and reported to increase primary bile acids while depleting secondary bile acids in the gut(*18*). Compared to untreated SPF mice, vancomycin-treated mice exhibited reduced levels of DCA in both feces (**Extended Data Fig. 9d**) and serum (**Extended Data Fig. 9e**) and reduced diABZI-induction of IFN-β (**Extended Data Fig. 9f**) and IL-6 (**Extended Data Fig. 9g**), demonstrating antibiotic depletion of microbiota and secondary bile acids impaired STING activation *in vivo*.

As vancomycin has been reported to deplete secondary bile acid-producing microbiota species such as *Clostridium scindens* (*18*), we evaluated whether *C. scindens* impacts STING activation *in vivo* compared to *Clostridium sporogenes*, which does not contain the *bai* operon responsible for producing secondary bile acids(*6, 64*),. To investigate whether DCA-producing microbiota

species modulates STING activation *in vivo*, we colonized antibiotic-treated mice with *C. scindens* or *C. sporogenes* and evaluated their effects on type I IFN activation and antitumor activity. We found that *C. scindens*, which was able to convert CA to DCA *in vitro* (**Extended Data Fig. 9h**), but not *C. sporogenes*, promoted IFN-β induction in vancomycin-treated mice stimulated with STING agonist diABZI (**Extended Data Fig. 9i**). To examine whether *C. scindens* enhances the antitumor efficacy of STING agonists, we colonized antibiotic cocktail or vancomycin-treated mice with bacteria and administered intratumoral injections of diABZI in the B16F10 tumor model (**Fig.5f**). Mice colonized with *C. scindens*, but not *C. sporogenes*, showed significantly reduced tumor growth following diABZI treatment in either antibiotic cocktail (**Fig. 5g, Supplementary Fig. 2a**) or vancomycin **(Fig. 5h, Supplementary Fig. 2b**) treated mice. Notably, *C. scindens*, but not *C. sporogenes*, also promoted the antitumor activity of a single diABZI injection (**Fig. 5i, Extended Data Fig. 10a, b**) and was inactive alone (**Fig. 5i)**. Flow cytometry analysis of TILs revealed that *C. scindens*, but not *C. sporogenes* supplementation significantly increased NK1.1□CD45$^+$ cells (**Fig. 5j, k, Extended Data Fig.10c**), CD3□CD45$^+$ cells (**Fig. 5l**)**,** and activated Sca-1$^+$CD8$^+$ T cells (**Extended Data Fig. 10d**), Ki67$^+$CD8$^+$ T cells (**Extended Data Fig. 10e**), and PD-1$^+$CD8$^+$ T cells (**Extended Data Fig. 10f**), similar to mice co-injected with DCA and diABZI (**Fig. 4g-j, Extended Data Fig. 8c**). Together, these findings demonstrate that DCA-producing microbiota such as *C. scindens* can synergize with STING agonists to enhance type I interferon signaling and antitumor immunity *in vivo*.

The diversity of microbiota species and metabolites represents a major challenge for functional studies in health, disease and therapy response. While previous studies have shown the microbiota and secondary bile acids can stimulate type I interferon signaling(*14*), how DCA enhanced type I interferon signaling was unclear. Using a reverse chemical microbiology

approach(*65*), our proteomic analysis of microbiota-derived bile acid protein targets revealed a previously unpredicted functional interaction between DCA and the innate immune sensor STING. Through cell signaling, cellular photocrosslinking and cryo-EM studies, we demonstrated that DCA, but not its primary bile acid precursor CA, binds to the transmembrane dimer-dimer interface of STING and promotes its oligomerization and stimulation of immune signaling. Furthermore, our studies show DCA and DCA-producing microbiota species can promote type I interferon signaling and antitumor activity of STING agonists *in vivo*. Of note, secondary bile acids alone have been shown to suppress antitumor immunity and promote cancer progression(*18-21*). However, our studies establish an unpredicted functional link between microbiota-derived secondary bile acids such as DCA and STING signaling, which suggest that the microbiota and bile acid composition of patients may impact the efficacy of STING-targeted therapies for antitumor immunity(*45*). Furthermore, as highly potent synthetic STING agonists exhibit significant on-target and cell type-dependent toxicities(*45*), the synergistic activity of DCA and DCA-producing microbiota species we observe with lower doses of STING agonists may be leveraged to improve the efficacy of these immunotherapies for cancer and other diseases(*7, 14, 15, 29, 43, 66*).

References and Notes

1. A. F. Hofmann, L. R. Hagey, Key discoveries in bile acid chemistry and biology and their clinical applications: history of the last eight decades. *J Lipid Res* **55**, 1553-1595 (2014).
2. R. A. Quinn *et al.*, Global chemical effects of the microbiome include new bile-acid conjugations. *Nature* **579**, 123-129 (2020).

3. E. C. Gentry *et al.*, Reverse metabolomics for the discovery of chemical structures from humans. *Nature* **626**, 419-426 (2023).

4. I. Mohanty *et al.*, The underappreciated diversity of bile acid modifications. *Cell* **187**, 1801-1818 e1820 (2024).

5. T. H. Won *et al.*, Host metabolism balances microbial regulation of bile acid signalling. *Nature* **638**, 216-224 (2025).

6. C. G. Buffie *et al.*, Precision microbiome reconstitution restores bile acid mediated resistance to Clostridium difficile. *Nature* **517**, 205-208 (2015).

7. Y. Sato *et al.*, Novel bile acid biosynthetic pathways are enriched in the microbiome of centenarians. *Nature* **599**, 458-464 (2021).

8. Q. Nie *et al.*, Gut symbionts alleviate MASH through a secondary bile acid biosynthetic pathway. *Cell* **187**, 2717-2734.e2733 (2024).

9. I. Mohanty *et al.*, The changing metabolic landscape of bile acids – keys to metabolism and immune regulation. *Nature Reviews Gastroenterology & Hepatology* **21**, 493-516 (2024).

10. J. Lin *et al.*, A microbial amino-acid-conjugated bile acid, tryptophan-cholic acid, improves glucose homeostasis via the orphan receptor MRGPRE. *Cell* **188**, 4530-4548.e4525 (2025).

11. J. Yang *et al.*, Structure-guided discovery of bile acid derivatives for treating liver diseases without causing itch. *Cell* **187**, 7164-7182.e7118 (2024).

12. M. H. Lee *et al.*, How bile acids and the microbiota interact to shape host immunity. *Nature Reviews Immunology* **24**, 798-809 (2024).

13. S. Lindner *et al.*, Altered microbial bile acid metabolism exacerbates T cell-driven inflammation during graft-versus-host disease. *Nature Microbiology* **9**, 614-630 (2024).

14. E. S. Winkler *et al.*, The Intestinal Microbiome Restricts Alphavirus Infection and Dissemination through a Bile Acid-Type I IFN Signaling Axis. *Cell* **182**, 901-918 e918 (2020).

15. M.-M. Hu *et al.*, Virus-induced accumulation of intracellular bile acids activates the TGR5-β-arrestin-SRC axis to enable innate antiviral immunity. *Cell Research* **29**, 193-205 (2019).

16. T. Hagan *et al.*, Antibiotics-Driven Gut Microbiome Perturbation Alters Immunity to Vaccines in Humans. *Cell* **178**, 1313-1328.e1313 (2019).

17. Q. Qu *et al.*, Lithocholic acid phenocopies anti-ageing effects of calorie restriction. *Nature* **643**, 192-200 (2025).

18. C. Ma *et al.*, Gut microbiome–mediated bile acid metabolism regulates liver cancer via NKT cells. *Science* **360**, eaan5931 (2018).

19. T. Fu *et al.*, FXR Regulates Intestinal Cancer Stem Cell Proliferation. *Cell* **176**, 1098-1112 e1018 (2019).

20. J. Cong *et al.*, Bile acids modified by the intestinal microbiota promote colorectal cancer growth by suppressing CD8+ T cell effector functions. *Immunity* **57**, 876-889.e811 (2024).

21. S. K. Varanasi *et al.*, Bile acid synthesis impedes tumor-specific T cell responses during liver cancer. *Science* **387**, 192-201 (2025).

22. W.-B. Jin *et al.*, Microbiota-derived bile acids antagonize the host androgen receptor and drive anti-tumor immunity. *Cell* **188**, 2336-2353.e2338 (2025).

23. M. Makishima *et al.*, Identification of a nuclear receptor for bile acids. *Science* **284**, 1362-1365 (1999).

24. D. J. Parks *et al.*, Bile acids: natural ligands for an orphan nuclear receptor. *Science* **284**, 1365-1368 (1999).

25. Y. Kawamata *et al.*, A G Protein-coupled Receptor Responsive to Bile Acids *. *Journal of Biological Chemistry* **278**, 9435-9440 (2003).

26. S. Hang *et al.*, Bile acid metabolites control TH17 and Treg cell differentiation. *Nature* **576**, 143-148 (2019).

27. C. Campbell *et al.*, Bacterial metabolism of bile acids promotes generation of peripheral regulatory T cells. *Nature* **581**, 475-479 (2020).

28. X. Song *et al.*, Microbial bile acid metabolites modulate gut RORgamma(+) regulatory T cell homeostasis. *Nature* **577**, 410-415 (2020).

29. W. Li *et al.*, A bacterial bile acid metabolite modulates Treg activity through the nuclear hormone receptor NR4A1. *Cell Host & Microbe* **29**, 1366-1377.e1369 (2021).

30. D. Paik *et al.*, Human gut bacteria produce TH17-modulating bile acid metabolites. *Nature* **603**, 907-912 (2022).

31. Q. Qu *et al.*, Lithocholic acid binds TULP3 to activate sirtuins and AMPK to slow down ageing. *Nature* **643**, 201-209 (2025).

32. E. R. Forster, X. Yang, A. K. Tai, H. C. Hang, A. Shen, Identification of a Bile Acid-Binding Transcription Factor in Clostridioides difficile Using Chemical Proteomics. *ACS Chemical Biology* **17**, 3086-3099 (2022).

33. B. Liu *et al.*, Chemoproteomic Profiling Reveals the Mechanism of Bile Acid Tolerance in Bacteria. *ACS Chemical Biology* **17**, 2461-2470 (2022).

34. X. Yang, X. Zhao, V. Chen, H. C. Hang, Chemical proteomic analysis of bile acid-protein targets in Enterococcus faecium. *RSC Chemical Biology* **3**, 1397-1402 (2022).

35. X. Yang, K. R. Stein, H. C. Hang, Anti-infective bile acids bind and inactivate a Salmonella virulence regulator. *Nature Chemical Biology* **19**, 91-100 (2023).

36. S. Zhuang, Q. Li, L. Cai, C. Wang, X. Lei, Chemoproteomic Profiling of Bile Acid Interacting Proteins. *ACS Cent Sci* **3**, 501-509 (2017).

37. S. Y. Park, S. B. Kim, J. Wan, F. Felice, K. H. Yi, Lipolytic agents for submental fat reduction: Review. *Skin Research and Technology* **30**, e13601 (2024).

38. H. Ishikawa, G. N. Barber, STING is an endoplasmic reticulum adaptor that facilitates innate immune signalling. *Nature* **455**, 674-678 (2008).

39. D. L. Burdette *et al.*, STING is a direct innate immune sensor of cyclic di-GMP. *Nature* **478**, 515-518 (2011).

40. G. N. Barber, STING: infection, inflammation and cancer. *Nature Reviews Immunology* **15**, 760-770 (2015).

41. C. Zhang *et al.*, Structural basis of STING binding with and phosphorylation by TBK1. *Nature* **567**, 394-398 (2019).

42. S. Yum, M. Li, Y. Fang, Z. J. Chen, TBK1 recruitment to STING activates both IRF3 and NF-κB that mediate immune defense against tumors and viral infections. *Proceedings of the National Academy of Sciences of the United States of America* **118**, e2100225118 (2021).

43. F. Humphries *et al.*, A diamidobenzimidazole STING agonist protects against SARS-CoV-2 infection. *Sci Immunol* **6**, eabi9002 (2021).

44. B. A. Flood, E. F. Higgs, S. Li, J. J. Luke, T. F. Gajewski, STING pathway agonism as a cancer therapeutic. *Immunological Reviews* **290**, 24-38 (2019).

45. E. N. Chin, A. Sulpizio, L. L. Lairson, Targeting STING to promote antitumor immunity. *Trends in cell biology* **33**, 189-203 (2023).

46. J. M. Ramanjulu *et al.*, Design of amidobenzimidazole STING receptor agonists with systemic activity. *Nature* **564**, 439-443 (2018).

47. E. N. Chin *et al.*, Antitumor activity of a systemic STING-activating non-nucleotide cGAMP mimetic. *Science* **369**, 993-999 (2020).

48. B. S. Pan *et al.*, An orally available non-nucleotide STING agonist with antitumor activity. *Science* **369**, eaba6098 (2020).

49. D. Lu *et al.*, Activation of STING by targeting a pocket in the transmembrane domain. *Nature* **604**, 557-562 (2022).

50. J. Li *et al.*, Activation of human STING by a molecular glue-like compound. *Nature Chemical Biology* **20**, 365-372 (2024).

51. B. C. Zhang *et al.*, Cholesterol-binding motifs in STING that control endoplasmic reticulum retention mediate anti-tumoral activity of cholesterol-lowering compounds. *Nat Commun* **15**, 2760 (2024).

52. I. Ford *et al.*, Defining STING-sterol interactions with chemoproteomics. *RSC Chemical Biology*, (2025).

53. L. Jin *et al.*, Identification and characterization of a loss-of-function human MPYS variant. *Genes & Immunity* **12**, 263-269 (2011).

54. F. Humphries *et al.*, Targeting STING oligomerization with small-molecule inhibitors. *Proceedings of the National Academy of Sciences of the United States of America* **120**, e2305420120 (2023).

55. J. Li *et al.*, Activation of human STING by a molecular glue-like compound. *Nat Chem Biol* **20**, 365-372 (2024).

56. A. T. Hansel-Harris, A. F. Tillack, D. Santos-Martins, M. Holcomb, S. Forli, Docking guidance with experimental ligand structural density improves docking pose prediction

and virtual screening performance. *Protein science : a publication of the Protein Society* **34**, e70082 (2025).

57. H. Hao *et al.*, Farnesoid X Receptor Regulation of the NLRP3 Inflammasome Underlies Cholestasis-Associated Sepsis. *Cell Metabolism* **25**, 856-867.e855 (2017).

58. L. Corrales *et al.*, Direct Activation of STING in the Tumor Microenvironment Leads to Potent and Systemic Tumor Regression and Immunity. *Cell reports* **11**, 1018-1030 (2015).

59. W. J. Ho, E. M. Jaffee, L. Zheng, The tumour microenvironment in pancreatic cancer — clinical challenges and opportunities. *Nature Reviews Clinical Oncology* **17**, 527-540 (2020).

60. K. C. Lam *et al.*, Microbiota triggers STING-type I IFN-dependent monocyte reprogramming of the tumor microenvironment. *Cell* **184**, 5338-5356.e5321 (2021).

61. Y. Shi *et al.*, Intratumoral accumulation of gut microbiota facilitates CD47-based immunotherapy via STING signaling. *J Exp Med* **217**, (2020).

62. W. Si *et al.*, Lactobacillus rhamnosus GG induces cGAS/STING- dependent type I interferon and improves response to immune checkpoint blockade. *Gut* **71**, 521-533 (2022).

63. Y. Gao *et al.*, Fusobacterium nucleatum enhances the efficacy of PD-L1 blockade in colorectal cancer. *Signal Transduct Target Ther* **6**, 398 (2021).

64. M. Funabashi *et al.*, A metabolic pathway for bile acid dehydroxylation by the gut microbiome. *Nature* **582**, 566-570 (2020).

65. X. Yang, H. C. Hang, Chemical genetic approaches to dissect microbiota mechanisms in health and disease. *Science* **386**, eado8548 (2024).

66. M. F. Gulen *et al.*, cGAS-STING drives ageing-related inflammation and neurodegeneration. *Nature* **620**, 374-380 (2023).

5

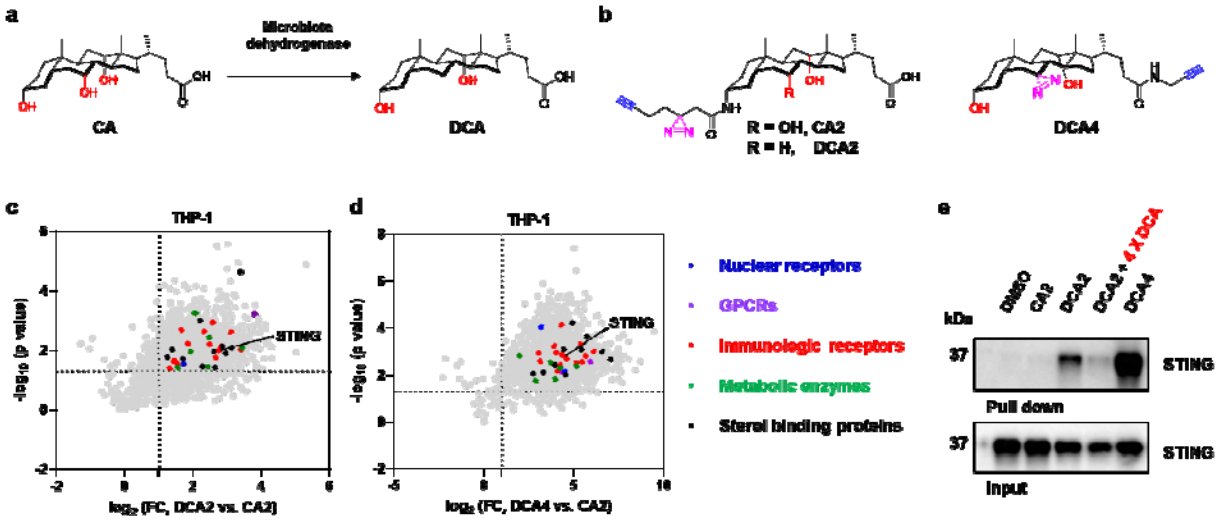

Figure 1. Proteome-wide mapping of DCA-interacting proteins in mammalian cell reveals DCA-STING interaction. (a) DCA is synthesized from CA by gut microbiota dehydrogenase. (b) Chemical structure of bile acid photoaffinity probes. (c, d) DCA2 (25 μM) and DCA4 (25 μM) bile acid photoaffinity reporters enrich more proteins compared to CA2 in THP-1 cells. STING is one of proteins that are selectively enriched by DCA photoaffinity reporters. Other DCA-enriched proteins are highlighted by different colors. (e) Validation of bile acid-STING interaction in THP-1 by reverse western blot. THP-1 cells were treated with bile acid photoaffinity reporters (25 μM) with or without excess of DCA for 0.5 h, followed by 365-nm light irradiation. The labeled proteins were reacted with az-biotin and enriched with streptavidin beads ('pulldown'). Equal loading was validated by immunoblotting of input samples before enrichment ('input').

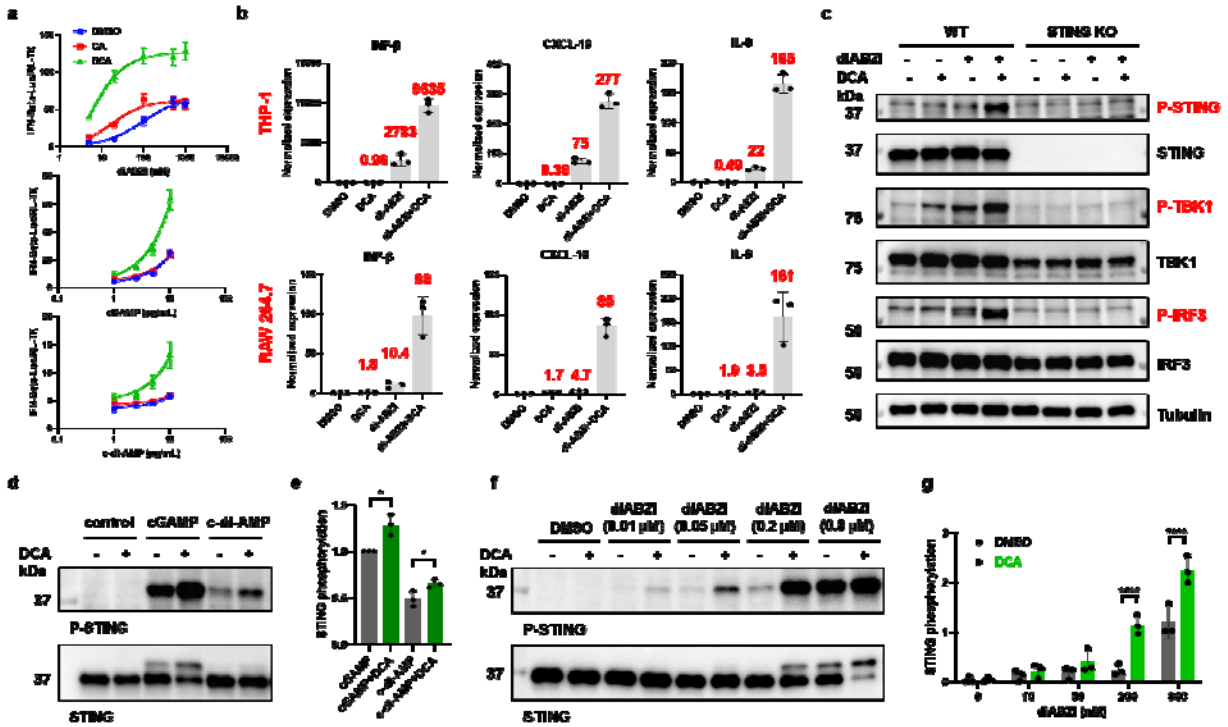

Figure 2. Bile acids promote STING activation ex vivo. (a) HEK293T transfected with pMSCV-hygro-STING, IFN-Beta_pGL3 (a luciferase reporter plasmid under control of the IFN-β promoter) and pRL-TK control plasmid were treated with different doses of STING agonists (diABZI, cGAMP, c-di-AMP) in presence or absence of DCA and CA (50 μM) (For diABZI, *n* = 5, for cGAMP and c-diAMP, *n* = 3, biologically independent samples). (b) qRT-PCR analysis of INF-β, CXCL-10, IL-6 in THP-1 and RAW264.7 cells treated with diABZI (50 nM for THP-1, 200 nM for RAW264.7) and DCA (50 μM) alone or together for 4 hours (*n* = 3 biologically independent samples). (c) Western blot analysis of cell lysates from THP-1 cells (WT and STING KO) treated with diABZI (50 nM) and DCA (50 μM) alone or together for 4 hours. (d) Western blot analysis of cell lysates from Human PBMCs treated with STING agonists (cGAMP (5 μg/mL), c-di-AMP (5 μg/mL), transfected with lipo2000 (1 μg/μL)) and DCA (50 μM) alone or together for 1 hours. (f) Western blot analysis of cell lysates from Human PBMCs treated with different concentration of diABZI with or without DCA (50 μM) for 2

hours. (e, g) Quantification of phosphorylated STING by grayscale analysis (p-STING/STING) (n = 3 biologically independent samples). For e, data were analyzed by unpaired two-sided t-test. for g, a two-way ANOVA followed by Sidak's multiple comparisons test was used to calculate adjusted P values. *P < 0.05, ****P < 0.0001.

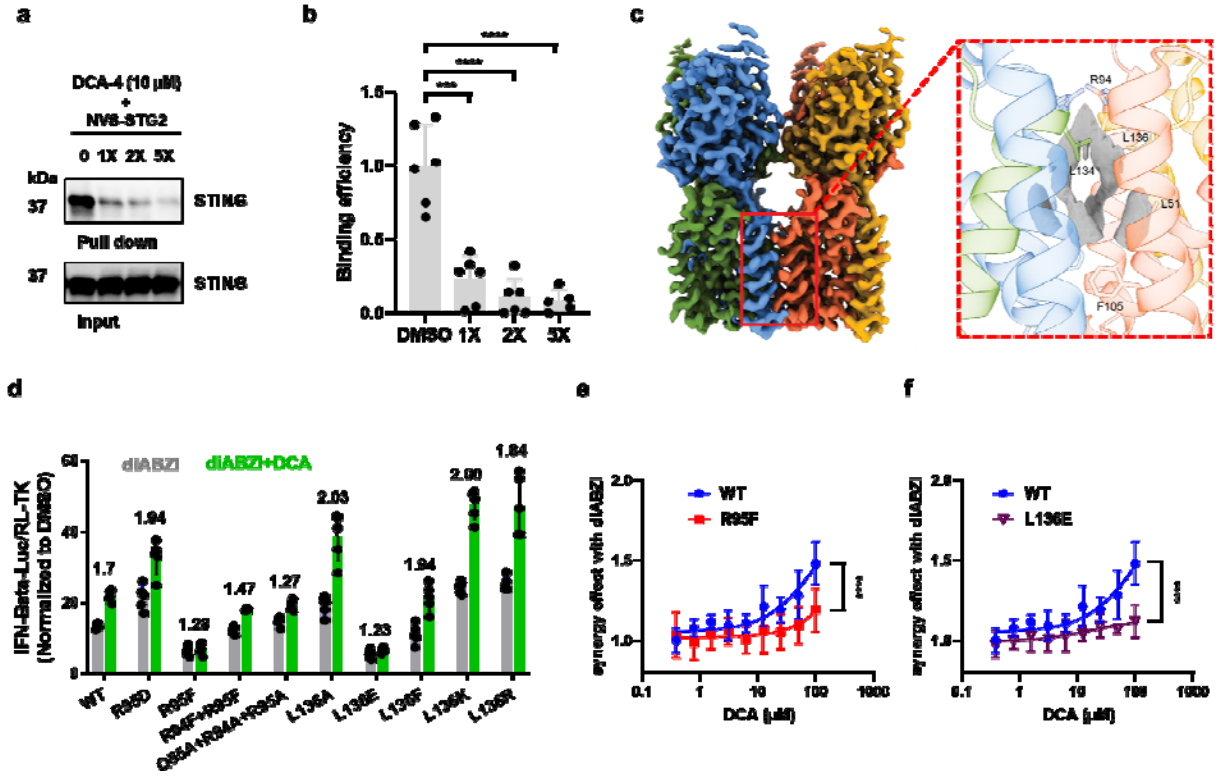

Figure 3. Bile acids target at STING dimer-dimer interface. (a) HEK293T transfected with pMSCV-hygro-STING were treated with DCA-4 (10 μM) in presence of different concentrations of NVS-STG2 for 30 mins at 37 ^{o}C, followed by 365-nm light irradiation. The labeled proteins in cell lysis were reacted with az-biotin and enriched with streptavidin beads ('pulldown'). Equal loading was validated by immunoblotting of input samples before enrichment ('input'). (b) Quantification of binding efficiency in A by grayscale analysis (pull down/input) (n =□5 - 6 biologically independent samples.). Data were analyzed by unpaired two-sided t-test. (c) High-resolution cryo-EM map of the two STING dimer with highlight of dimer-dimer interface

molecular density. (d-f) HEK293T transfected with pMSCV-hygro-STING (WT and mutations), IFN-Beta_pGL3 and pRL-TK control plasmid were treated with diABZI (20 nM) in presence or absence of DCA (n = 5 biologically independent samples). A two-way ANOVA followed by Sidak's multiple comparisons test was used to calculate adjusted P values. *P < 0.05, **P < 0.01, ***P < 0.001, ****P < 0.0001.

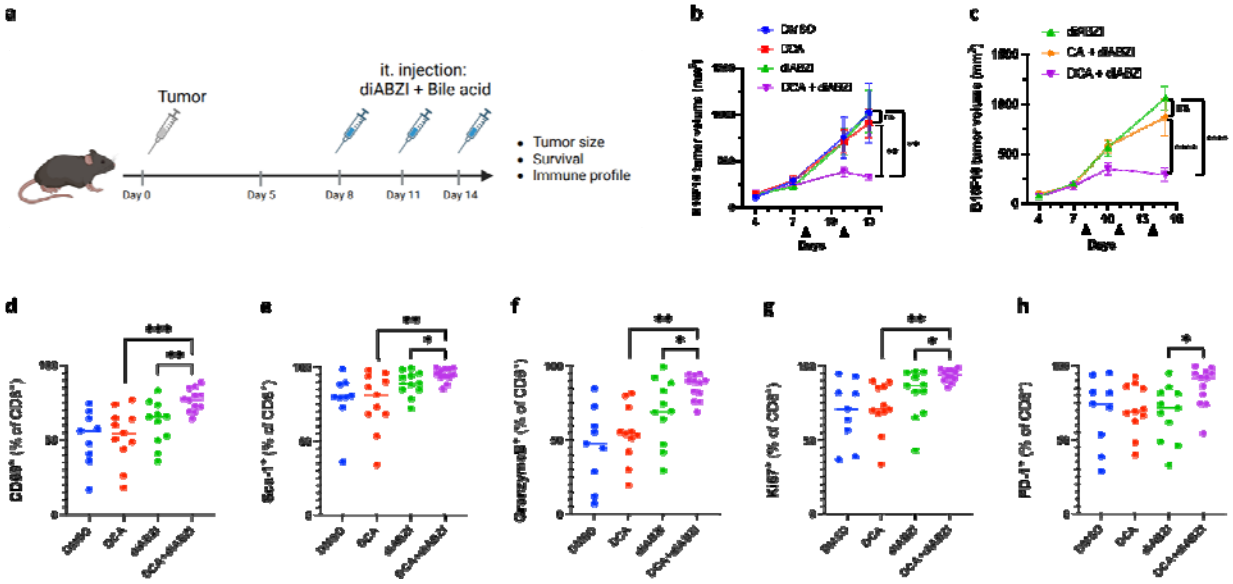

Figure 4. DCA boost STING-targeted antitumor immunity *in vivo*. (a) Schematic of the tumor model. SPF mice were subcutaneously implanted with tumor cells. Tumor volume measurements began on day 4, when tumors reached approximately 50–100 mm³. Intratumoral (i.t.) injections of diABZI and/or bile acids were administered every two days starting on day 8, when tumors reached ~250 mm³. (b) B16-F10 melanoma tumor growth in mice treated i.t. with vehicle (DMSO), DCA, diABZI, or the combination (DCA + diABZI). (c) B16-F10 tumor growth in mice treated i.t. with diABZI alone or in combination with CA or DCA. (d-h) Quantification of tumor-infiltrating CD8 T cells expressing Sca-1 (d) CD69 (e) Granzyme B (f) Ki-67 (g), or PD-1 (h) in B16-F10 tumors from mice treated with DMSO, DCA, diABZI, or the combination. Tumors were harvested 2 days after a single i.t. injection. Data in b **and c**

represent mean ± SEM and were analyzed using a mixed-effects model with Tukey's multiple comparisons post hoc test (n = 8 mice per group). Arrowheads indicate the days of i.t. injection. Data in d–h were pooled from two independent experiments, represent mean ± SEM, and were analyzed using an unpaired *t*-test (n = 9–12 mice per group). Each symbol represents one mouse. *P < 0.05, **P < 0.01, ***P < 0.001, ****P < 0.0001; ns, not significant.

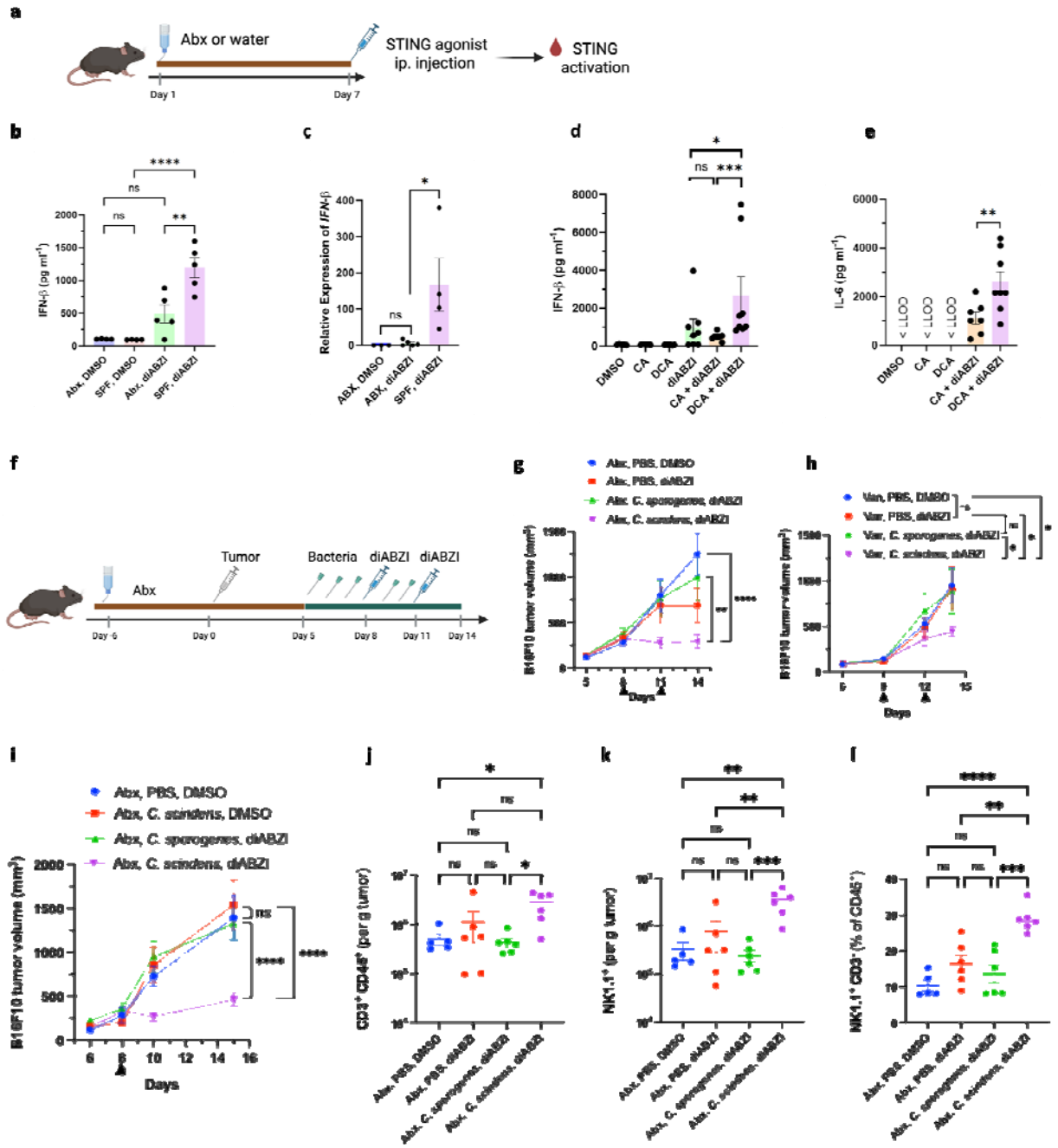

Figure 5. Microbiota producing DCA promote STING-mediated Type 1 signaling and antitumor response. (a-c) Mice were treated with or without an antibiotic cocktail (Abx) for 1 week. On Day 7, mice were received i.p. injection of diABZI. Serum IFN-β was quantified by ELISA (b), and cecal *Ifnb1* gene expression was analyzed by qPCR (c). (d, e) Mice were treated with Abx for 1 week, then i.p. injected on Day 7 with diABZI in the presence or absence of bile

acids. Four hours post-injection, serum IFN-β (d) and IL-6 (e) levels were measured by ELISA. (f) Schematic of the tumor growth model used for panels g and h. (g–h) B16F10 tumor growth curves in mice treated with Abx (g) or vancomycin (h). Mice received Abx or vancomycin for 10 days. On day 5 post-tumor implantation, Abx or vancomycin treatment was stopped, and mice began daily oral gavage with PBS, *C. sporogenes*, or *C. scindens*. diABZI was administered via it. injection on days 8 and 11. (i-l), B16F10 tumor growth (i) and flow cytometry analysis (j-l) in Abx-treated mice gavaged with indicated bacteria and receiving a single diABZI injection. Frequency (j) and absolute number (k) of tumor-infiltrating $NK1.1^+$ $CD3^-$ cells, and number of tumor-infiltrating $CD3^+$ $CD45^+$ cells (l). Data in b-e: n = 5-8 mice per group. Data are presented as mean ± SEM and analyzed by unpaired two-tailed t-test. Data ing and i: n = 8 mice per group. Data in h: n = 5 mice per group. Data g-i represent mean ± SEM and were analyzed using a mixed-effects model with Tukey's multiple comparisons post hoc test. Data in j-l: n = 5–6 mice per group, represent mean ± SEM and were analyzed using unpaired two-tailed *t*-test. *P < 0.05, **P < 0.01, ***P < 0.001, ****P < 0.0001; ns, not significant.

Methods:

Cell culture

HEK293T, HT-29, HeLa, THP-1, RAW264.7, B16-F10, MC-38, Panc02 were obtained from ATCC. PBMCs were fresh isolated from donor. HEK293T, HT-29, HeLa, RAW264.7, B16-F10, MC-38, Panc02 cells were cultured in DMEM (Gibco) supplemented with 10% FBS (GE Healthcare HyClone) and 100 μg ml^{-1} penicillin–streptomycin (Thermo Fisher Scientific). THP-1 and hPMBCs were cultured in RPMI supplemented with 10% FBS. All cells were cultured in a 37 °C incubator with 5% CO_2. Cells were also routinely cultured without antibiotics to ensure no bacterial infection.

Bacterial culture

C. scindens ATCC 35704 and *C. sporogenes* ATCC 15579 were obtained from C.-J. Guo lab (Weill Cornell Medical School). Bacteria were cultured in Modified Reinforced Clostridial broth (ATCC Medium 2107) and/or TSAB (Tryptic Soy Agar supplemented with 5% Horse Blood, 1% L-Cysteine hydrochloride, and 0.1% Vitamin K3) within an anaerobic chamber (Coy Laboratory Products) at 37 °C for 24 to 48 hours(*67*). Mice were administered 1×10^8 CFU of bacteria daily via oral gavage.

Animals

Specific pathogen-free, seven-week-old male and female C57BL/6 (B6, 000664) mice were obtained from the Scripps Rodent Breeding Colony. The mice were housed in autoclaved cages with SaniChip bedding and nest-building enrichment on a 12-hour light/dark cycle. They were provided gamma-irradiated chow (LabDiet 5053) and sterile drinking water ad libitum. All animal care and experimental procedures were conducted in accordance with NIH guidelines and were approved by the Institutional Animal Care and Use Committee at Scripps Research (Protocol AUP-21-095).

Chemical reagents

Compounds were purchased and used directly without further purification. Catalog is shown as below: diABZI (99.84%, MCE, HY-112921B), MSA-2 (≥98%, Cayman, 30140), c-di-AMP (≥ 95% by LC/MS, InvivoGen, tlrl-nacda), 2’3’-cGAMP (≥ 95% by LC/MS, InvivoGen, tlrl-nacga23), c-di-GMP (≥ 95% by LC/MS, InvivoGen, tlrl-nacdg), C53 (≥98%, Cayman, 37354), cholic acid (97%, Alfa Aesar, A11267), NVS-STG2 (98%, MCE, HY-157214), DMXAA (≥98%, Cayman, 14617), BB-Cl-Amidine (≥95%, MCE, hy-111347), single-stranded template DNA (HT-DNA) (sigma, D7656), deoxycholic acid (≥98%, HPLC, Sigma, D2510-100G),

chenodeoxycholic acid (>98%, Abcam, ab142267), lithocholic acid (≥95%, Sigma, L6250-25G), ursodeoxycholic aicd (99%, BTC, 123710-5g), Alloisolithocholic Acid (≥95%, Cayman, 29542), TCA (≥97%, sigma, 86339-1G), GCA (≥95%, SC-218574A), TDCA (SC-253596), GDCA (≥97%, HPLC, sigma, G9910-1G), TCDCA (99%, spectrum, T3925), GCDCA (spectrum, G3389), PEG400 (MCE, HY-Y0873A), Az-biotin was purchased from Sigma-Aldrich (762024).

Photoaffinity probe cell treatments

THP-1 cells were maintained in RPMI 1640 medium supplemented with 10% fetal bovine serum (FBS), ensuring a cell density below 1 × 10^6 cells/mL. To initiate treatment, cells were harvested by centrifugation at 200 g for 10 minutes, the supernatant was removed, and the pellet was resuspended in serum-free RPMI 1640 containing the bile acid reporter (CA2 -25 μM, DCA2-25 μM, DCA4-25 μM). The cells were then incubated for 30 minutes at 37 °C in a humidified atmosphere of 5% CO□. Following incubation, the medium was removed and replaced with cold DPBS, and the cells were placed in 15 cm dish on ice and exposed to UV light (365 nm) for 10 minutes and transferred into tubes. The suspensions were centrifuged again at 200 g for 10 minutes, and aspirated to remove the supernatant. Finally, the resulting cell pellets were flash-frozen in liquid nitrogen and stored at –80 °C until further processing.

Preparation of samples for chemoproteomic analysis

Chemoproteomic samples were prepared in biological duplicates for each condition using previously described procedures(*68*). Briefly, cell pellets were resuspended in 500 μl of cold DPBS and lysed via sonication (Branson Sonifier probe; 15 ms on, 40 ms off, 15% amplitude, 7 pulses). Protein concentrations were normalized to 2 mg/ml in 500 μl of ice-cold DPBS, using a DC Protein Assay (Bio-Rad), in 15-ml falcon tubes. The “click-chemistry cocktail” was then added to each lysate, consisting of tris[(1-benzyl-1H-1,2,3-triazol-4-yl)methyl]amine (TBTA,

final concentration: 100 µM), tris(2-carboxyethyl)phosphine (TCEP, final concentration: 1 mM), biotin-azide (final concentration: 100 µM), and $CuSO_4$ (final concentration: 1 mM). Samples were incubated at room temperature for 1 hour. Ice-cold 4:1 MeOH/$CHCl_3$ (2.5 ml) and ice-cold DPBS (1 ml) were added to each sample to quench the click reaction, followed by centrifugation (3,200 g, 4 °C, 10 min) to precipitate proteins. The precipitates were washed twice more with 4:1 MeOH/$CHCl_3$ and resuspended in 500 µl of 6 M urea in DPBS, along with 10 µl of 10% SDS. Protein reduction was performed by adding 50 µl of a freshly prepared 1:1 solution of TCEP (25 µl, 200 mM in DPBS) and K_2CO_3 (25 µl, 600 mM in DPBS), and incubating at 37 °C for 30 minutes. Following reduction, proteins were alkylated by adding 70 µl of freshly prepared iodoacetamide (400 mM in DPBS) and incubated for 30 minutes at room temperature in dark. After alkylation, 130 µl of 10% SDS was added to the samples, followed by dilution with 5.5 ml of DPBS. A 100 µl aliquot of 50% streptavidin agarose slurry (Thermo Fisher Scientific, 20349) was added to each tube, and samples were rotated for approximately 1.5 hours at room temperature to enrich probe-labeled proteins. The beads were then centrifuged down to tube bottom (750 *g*, 2 min, 4 °C) and washed once with 0.2% SDS in DPBS (5 min), twice with DPBS, once with water, and transferred to LoBind microcentrifuge tubes with 100 mM TEAB (pH 8.5).

Bound proteins were digested overnight with trypsin (Promega, V5111) in digestion buffer [100 ml, 100 mM TEAB (pH 8.5), 100 µM $CaCl_2$] at 37 °C. The resulting peptides were transferred to new tubes for each condition and labeled with the respective tandem mass tags (TMT; Thermo Fisher Scientific) 10plex reagents (8 µl, 20 µg/µl) for 1 h, quenched by hydroxylamine (6 µl, 5% *v*/*v*) for additional 15 min, acidified by formic acid (8 µl), and dried through SpeedVac vacuum concentrator. The dried peptides were redissolved in 0.1% TFA in H_2O, combined, and proceeded to be fractionated into 12 fractions by Pierce high pH Reversed-Phase Fractionation

Kit (Thermo Fisher Scientific, 84868) according to manufacturer's instructions. The fractions were pooled pairwise into 6 final fractions, dried, and stored at −80°C until mass spectrometry analysis.

LC-MS analysis of TMT samples

Proteomic samples were resuspended in MS sample buffer (20 µl, 5% acetonitrile, 0.1 % formic acid in water) prior to LC-MS analysis, following published methoeds(*68*). In short, 3 µl of each sample was loaded onto an Acclaim PepMap 100 precolumn (75 µm × 2 mm) and separated on an Acclaim PepMap RSLC analytical column (75 µm × 15 cm) using an UltiMate 3000 RSLCnano system (Thermo Fisher Scientific). Buffer A (0.1% formic acid in H_2O) and buffer B (0.1% formic acid in acetonitrile) were used in a 220-minute gradient at a flow rate of 300 µl/min. The gradient consisted of 2% buffer B for the first 10 minutes, a gradual increase to 30% buffer B over the next 192 minutes, 60% buffer B for 5 minutes, followed by a ramp to 95% buffer B for 1 minute, held for 5 minutes, then lowered back to 2% buffer B for 1 minute, and re-equilibrated for 6 minutes.

Eluents were analyzed using a Thermo Fisher Scientific Orbitrap Fusion Lumos mass spectrometer with a 3-second cycle time and a nano-LC electrospray ionization voltage of 2,000 V. Data were acquired with Xcalibur software (v4.1.50). MS1 spectra were captured with a scan range of 375–1,500 m/z, a maximum injection time of 50 milliseconds, and dynamic exclusion enabled (1 repeat, exclusion duration of 20 seconds). The resolution was set to 120,000 with an AGC target of 1×10^6. Peptides chosen for MS2 analysis were isolated with a quadrupole (isolation window of 1.6 m/z) and fragmented by collision-induced dissociation (CID) at 30% collision energy. Fragment ions were recorded in the ion trap (AGC target 1.8×10^4, maximum injection time of 120 ms). MS3 spectra were generated using high-energy collision-induced

dissociation (HCD) mode with 65% collision energy, and synchronous precursor selection (SPS) was set to 10 SPS ions in MS3 for TMT fragmentation.

Proteomic result analysis

Proteomic analysis was carried out using Proteome Discoverer (v2.4 or v3.0, Thermo Fisher Scientific) following previously established protocols(*68*). Peptide identification was conducted using the SEQUEST HT algorithm, precursor mass tolerance is 10 ppm and fragment mass tolerances is 0.6 Da, allowing for one missed cleavage. Variable modifications included oxidation (M, +15.994915), carbamidomethyl (C, +57.02146) and TMT-tag modifications (K and N-terminal, +229.1629) were used as fixed modifications. The spectral data were searched against the Homo sapiens proteome database (Uniprot, 2018; 42,358 sequences), applying a 1% false discovery rate (FDR) with Percolator. MS3 peptide quantification used a mass tolerance of 20 ppm, and channel abundances were normalized to the median signal intensity across all channels.

To ensure data reliability, proteins reported required at least two unique peptides. TMT ratios calculated in Proteome Discoverer were transformed using log2(x), and statistical significance of the ratios was assessed with two-tailed t-tests across two biological replicates (significance threshold set at $P < 0.05$). Detailed proteomics data are available in Supplementary Date S1.

Pull-down of STING by bile acid photoaffinity probes

From the bile acid photoaffinity probes-treated or control total cell lysates prepared as described above, 225 μL of each total cell lysates (~250 μg protein) was added with 25 μL of click chemistry reagents as a 10X master mix (Az-biotin: 0.1 mM, 10 mM stock solution in DMSO; tris(2-carboxyethyl)phosphine hydrochloride (TCEP): 1 mM, 50 mM freshly prepared stock solution in dH_2O; tris[(1-benzyl-1H-1,2,3-triazol-4-yl)methyl]amine (TBTA): (0.1 mM, 2 mM

stock in 4:1 t-butanol: DMSO); $CuSO_4$ (1 mM, 50 mM freshly prepared stock in dH_2O). Samples were mixed well and incubated at room temperature for 1 h. After incubation, samples were mixed with 1 mL cold methanol and incubated at -20 ℃ overnight. Sample proteins were precipitated at 18000 g for 15 min at 4 °C. After gently removing the aqueous layer, protein pellets were washed with 500 µL cold methanol three times, spinning down at 18000 g for 15 min at 4 °C, and liquid was gently decanted. After last wash, pellets were let air dried before being re-solubilized in 100 uL 4% SDS PBS with bath sonication. Solutions were then diluted with 300 µL PBS, spun down (18000 g, 10 min) to remove any particles. 20 µL of supernatant was kept for "input" before enrichment. The left supernatant was incubated with 20 µL PBS-T-washed High Capacity NeutrAvidin agarose (Pierce) (500 µL PBS-T-washed twice, 2500 g, 60 s) at room temperature for 1 h with end-to-end rotation. The agarose was washed with 500 µL of 1% SDS PBS 3 times, 500 µL of 1M Urea PBS 3 times, and 500 µL of PBS 3 times. Samples were boiled with 2X Laemmli buffer 95 °C for 5 min before being loaded onto a 4-20% Tris-HCl gel (Bio-Rad) for SDS-PAGE. Equal loading is validated by immunoblotting of input samples before enrichment ("Input").

Western Blot

Cells were lysed by lysis buffer (1% SDS, 20 mM HEPES, 150 mM NaCl, pH 7.4, protease inhibitor cocktail (Roche), phosphatase inhibitor cocktail (PhosSTOP, Roche), benzonase (1:1000)). The concentration of cell lysis was determined by BCA assay (Pierce™ BCA Protein Assay Kits) and normalized with lysis buffer. Samples were then boiling with 1× Laemmli buffer at 95 °C for 5 min and loaded onto a 4–20% Tris-HCl gel (Bio-Rad) for SDS-PAGE. Proteins were then transferred onto a 0.45-µm nitrocellulose membrane (Bio-Rad) with a Trans-Blot Turbo Transfer System (Bio-Rad) at 25 V for 30 min. The membrane was blocked with 5%

non-fat milk in PBS-T or Protein-Free Blocking Buffer (927-80003, LI-COR) (for detection of phosphorylated proteins) for 60 min. Corresponding antibody was added to the solution before incubating the membrane at 4 °C overnight. The membrane was washed with PBS-T three times and incubated with 1:10,000 anti-rabbit HPR (Abcam, ab97051) or anti-mouse HRP (Abcam, ab97023) in PBS-T with 5% non-fat milk at room temperature for 1 h. The membrane was washed with PBS-T three times and imaged with Clarity Western ECL substrate (Bio-Rad) and a ChemiDoc imaging System (Bio-Rad). Following antibodies were used as per the manufacturer's instructions. NR1H4 Polyclonal antibody (25055-1-AP, Proteintech); IRF-3 (D83B9) Rabbit mAb (4302, Cell signaling technology); Phospho-IRF-3 (Ser386) (E7J8G) XP® Rabbit mAb (37829, Cell signaling technology); TBK1/NAK (D1B4) Rabbit mAb (3504, Cell signaling technology); Phospho-TBK1/NAK (Ser172) (D52C2) XP® Rabbit mAb (5483, Cell signaling technology); STING (D2P2F) Rabbit mAb (13647, Cell signaling technology); Phospho-STING (Ser366) (E9A9K) Rabbit mAb (50907, Cell signaling technology); Tubulin (ab6046, Abcam).

RT-qPCR

THP-1 or RAW 264.7 cells were grown in 6-well plates to 90% confluency. Cells were then treated with DMSO, DCA, di-ABZI with indicated concentration for 4 hours. RNA was purified using RNeasy Plus Kit (Qiagen). cDNA was then synthesized from purified RNA with iScript advanced cDNA synthesis kit (BioRad). The cDNA was diluted ten times with nuclease-free water. qRT–PCR was performed with PowerUp SYBR Green Master Mix (Applied Biosystems), per the manufacturer's instructions. The expression of target genes was normalized to the expression of housekeeping gene ACTB. Following primers were used:

humanIFNβ

(5’-AAACTCATGAGCAGTCTGCA-3’+5’-AGGAGATCTTCAGTTTCGGAGG-3’)

humanIL6

(5’-ACTCACCTCTTCAGAACGAATTG-3’+5’-CCATCTTTGGAAGGTTCAGGTTG-3’)

humanCXCL10

(5’-GGTGAGAAGAGATGTCTGAATCC-3’+5’-GTCCATCCTTGGAAGCACTGCA-3’)

murineIFNβ

(5’-TCCGAGCAGAGATCTTCAGGAA-3’+5’-TGCAACCACCACTCATTCTGAG-3’)

murineIL6

(5’-AACGATGATGCACTTGCAGA-3’+5’-GAGCATTGGAAATTGGGGTA-3’)

murineCXCL10

(5’-CCAAGTGCTGCCGTCATTTTC-3’+ 5’-GGCTCGCAGGGATGATTTCAA-3’)

Dual Luciferase reporter assay

HEK293T cells were seeded in 96-well Flat Clear Bottom White Polystyrene TC-treated Microplates (Corning) at 30,000 cells per well. After 16 h, cells were transiently transfected with three plasmids, including pMSCV-hygro-STING (Addgene, 102598), IFN-Beta_pGL3 (Addgene, 102597), and pRL-TK (Promega, E2241) using Lipofectamine 3000 Transfection Reagent (Invitrogen, L3000-015). After 24□h, cells were treated with indicated compounds for another 24□h. Luminescence was detected after the addition of dual-luciferase reporter assay reagent (Promega, E1960), using a BioTek Synergy Neo2 Multi-Mode Microplate Reader with a 0.5□s integration time. Firefly luciferase luminescence normalized to the Renilla luciferase control is shown.

STING-GFP imaging

HeLa cells stably expressing STING-GFP were generated by lentivirus transduction and selected by puromycin and GFP cell sorting. Cells grown on glass coverslips were treated with indicated conditions. Cells were then rinsed with ice-cold 1x PBS for 3 times and fixed with 4% paraformaldehyde for 20 minutes. Post fixation, the cells were further washed with 1x PBS for 5 minutes 3 times. Cells were then permeabilized with 0.3% Triton-X in PBS for 20 minutes and washed again with 1x PBS for 5 minutes 3 times before mounting for imaging. DAPI in the mounting medium (VECTASHIELD, H-1800) is used as the counterstain. All incubations were conducted at room temperature unless otherwise specified. Mounted coverslips were imaged with Nikon C2+ confocal microscopy. Resulting images were analyzed with CellProfiler (pipeline provided).

STING-oligomerization

THP1 cells were seeded in 6-well plates at a density of 1 × 10□ cells/mL and incubated with 100 nM or 200 nM diABZI in presence or absence of 50 μM DCA for 2 hours. Following treatment, the cells were resuspended in lysis buffer containing 50 mM HEPES (pH 7.4), 150 mM NaCl, 5 mM MgCl□, 1 mM DTT, protease inhibitor cocktail (Roche), and phosphatase inhibitor cocktail (PhosSTOP, Roche). The cell suspension was incubated on ice for 15 minutes, followed by sonication for cell lysis. Lysates were then centrifuged at 1,000 g for 5 minutes to obtain the S1 supernatant. An equal volume of buffer containing 2% NP-40 was added to the supernatant. Protein samples were mixed with 20% glycerol and resolved using a 4–20% Criterion TGX stain-free gel (Bio-Rad). Samples were run in Tris-Glycine running buffer supplemented with 0.05% Coomassie Brilliant Blue G-250 at a constant voltage of 120 V for 30 minutes. Following the initial run, the buffer was exchanged for clear Tris-Glycine buffer to enhance contrast on the

gel, and the separation continued until the dye front reached the bottom. Proteins were then transferred to a nitrocellulose membrane via immunoblotting for further analysis. The samples were also denatured and run with SDS-PAGE for immunoblotting with the indicated antibodies.

Cryo-EM sample preparation

The gene for human STING (UniProtKB Q86WV6) was codon-optimized, synthesized, and cloned into the pEZT-BM expression vector. The C-terminal tail following residue 343 was replaced with a linker region and Strep-tag (GGGSGGGSGGSAWSHPQFEK). HEK293F cells were grown at 37 °C to a density of ~1 million cells/mL and transfected with 1 mg DNA and 3 mg PEI per liter of cells. After 72 hours, cells were harvested by centrifugation, resuspended in 20 mM Tris 7.4 + 150 mM NaCl (TBS buffer) with 1 mM PMSF and 0.5 mM TCEP, and lysed by sonication. The cell lysate was centrifuged at 3,000 g for 10 min, and the supernatant was further centrifuged at 186,000 g for 2 hours to isolate membranes. The membrane fraction was then stored at -80°C. Membrane fractions were homogenized and solubilized for 2 hours at 4 °C in TBS + 1% DDM, 0.2% CHS, 1 mM PMSF, 0.5 mM TCEP, and 1 mM $CaCl_2$, then subsequently clarified via centrifugation at 186,000 g for 40 min. STING protein was affinity-purified from solubilized membranes with Strep-Tactin XT 4Flow (IBA) resin. Protein was eluted with Buffer BXT (IBA), and eluted protein was subjected to gel-filtration using a Superdex 200 Increase 10/300 GL column (Cytiva) in SEC buffer (TBS + 0.02% DDM, 0.004% CHS, 100 µM DCA, and 0.5 mM TCEP). SEC-purified STING was diluted to ~5 µM and incubated with 30 µM 2’3’-cGAMP (InvivoGen) and 30 µM C53 (Cayman) at 4 °C overnight, after which the sample was concentrated to ~8 mg/mL. 3 µL of sample was applied to glow-discharged UltrAuFoil 1.2/1.3 300-mesh grids (Quantifoil) before being blotted and plunge-frozen into liquid ethane using a Vitrobot Mark IV (Thermo Fisher).

Cryo-EM data collection and processing

A total of 5839 cryo-EM micrographs were collected on a 200 kV Glacios 2 microscope equipped with a Falcon 4i detector (Thermo Fisher) at a nominal magnification of 190,000x

resulting in a pixel size of 0.718 Å. Data were collected with EPU (Thermo Fisher) with an approximate dose of 45 e/Å2 and a nominal defocus range of -0.6 to -1.5 µm. Micrographs were aligned using Patch Motion Correction and CTF estimation was done by Patch CTF in Cryosparc Live(*69*). Micrographs with CTF fits lower than 8 Å were discarded, and all further data processing was done with Cryosparc. Blob picker was initially used on a subset of 300 micrographs to generate 2D classes to be used as templates for template picking for the full dataset. Picked particles were subjected to multiple rounds of 2D classification to remove false positives. Heterogeneous refinement, using PDB 7SII low-pass filtered to 20 Å as an initial model, was used to select a final subset of 285k particles. Non-uniform refinement(*70*) and local refinement with a mask around two STING protomers yielded a final map at 2.9 Å resolution using C2 symmetry and 3.0 Å with C1 symmetry. PDB 7SII was docked into the C2 map using UCSF ChimeraX(*71*). The model was manually adjusted using Coot (*72, 73*) and subjected to real-space refinement in Phenix(*74*). Structural figures were made using UCSF ChimeraX.

Docking Method

The STING tetramer structure was protonated using Reduce(*75*) and prepared for docking using Meeko (https://github.com/forlilab/Meeko) to assign atom types and Gasteiger partial charges and convert to a PDBQT file. Grid maps were initially calculated with AutoGrid4 with a box size of 32 □, 34 □, 30 □ (0.375 □ grid spacing) and with the box center at 112 □, 116□, 92 □. Ligand files were made into 3-dimensional SD Files from SMILES using Scrubber (https://github.com/forlilab/scrubber), then converted to PDBQTs with Meeko.

The five different ligands (Cholic acid, DCA, Iso-DCA, Iso-LCA, and UDCA) were docked with STING using a custom docking engine employing a search method similar to AutoDock-Vina (Monte-Carlo global search, L-BFGS local search) with the AutoDock4.2 force field and affinity

grid maps modified using our CryoXKit software (manuscript submitted) to include guidance from the C2-symmetric cryo-EM density.

For creating the density cloud representations of the ligands during docking, we add a Boltzmann weight, $\exp(-E_n/kT)$, based on the energy E_n of each accepted pose to a grid map at the locations of each atom. This is done separately for each Monte-Carlo run and then subsequently summed into a single map by renormalizing each run's map points with the overall best energy's Boltzmann weight $\exp(-E_{best}/kT)$ Subsequently, a Gaussian convolution with a width of (1.58/2) □ is performed and the resulting grid map is output as an MRC file.

ELISA

Mice were pre-treated with either a broad-spectrum antibiotic cocktail (5□g/L streptomycin, 1□g/L colistin sulfate, and 1□g/L ampicillin) (*68, 69*) or vancomycin (0.5g/L) administered in drinking water for one week prior to treatment. On Day 7, mice were ip. injected with STING agonists and/or bile acids. The following doses were used per injection: CA or DCA – 20 mg/kg; diABZI – 1 mg/kg; and c-di-AMP – 1 or 5 mg/kg. For the CA-bacteria experiment, the antibiotic cocktail was replaced with 1mM cholic acid sodium salt (Thermo Fisher, 361-09-1), administered in drinking water in parallel with daily oral gavage of bacteria. Blood samples were collected via retro-orbital bleeding 4 hours post-treatment, and serum was isolated by centrifugation. IFN-β land IL-6 levels were quantified using a mouse IFN-β ELISA kit (PBL Assay Science, 42400-1) and a mouse IL-6 ELISA kit (Thermos Fisher, KMC0061), following the manufacturer’s instructions.

LC-MS analysis of extracted bile acids.

Protocols were adapted from [1–3]. Fecal pellets were collected, weighed and transferred into tubes containing several 1 mm diameter beads (Cat. No. 11079110). Each sample was extracted three times with 400 µL cold LC-MS grade methanol, homogenized at 4 m/s for 30 s, and pooled. The combined supernatant (~1.2 mL) was incubated at –20 °C for 1–2 h to precipitate proteins, then centrifuged at ≥13,000 × g for 15 min at 4 °C. Serum samples were treated with 4 × volume of cold methanol. The mixture was vortexed and sonicated for 10 min. Proteins were precipitated at −20°C for 16 hours. Next, the proteins were centrifuged at 13,000 rpm for 15 min at 4°C. The clear supernatants were further subjected to LC-MS analysis.

Bile acid standards (CA and DCA) and bacterial culture extracts were analyzed using 1290 Infinity II LC/MSD system (Agilent) equipped with Zobrax SB-C18 Rapid resolution HT (2.1 × 50 mm,1.8 µm). Samples were run at flow rate 0.35 mL/min in mobile phase (A: water, 0.1% formic acid), room temperature and an eluent (B: acetonitrile, 0.1% formic acid) using following gradient: 0-1 min: 5% B, 1-8 min: 60-70% B, 8-9 min: 70-95% B, 9-11 min: 95% B, 11-12 min: 95-5% B. Selected ion abundance was collected with MSD API-ES in negative-ion SIM mode with target masses of CA (m/z = 407.2) and DCA (m/z = 391.2). Extracted intensities were analyzed by GraphPad Prism.

Tumor inoculation, measurements and treatments

Tumor cells were cultured for one week and split the day prior to harvesting for tumor inoculation. Cells were harvested using TrypLE Express (Invitrogen, 12604021), washed, and resuspended in cold phosphate-buffered saline (PBS), then counted using a hemocytometer. The cells were resuspended at 2× concentration in PBS on ice and subsequently diluted 1:1 with Matrigel Matrix (Corning, 356231). Animals were anesthetized with 2.5% isoflurane, and the right flank was shaved using hair clippers. Each animal was subcutaneously injected with 100 µL

of the cell suspension into the mid-right flank. The final number of injected cells per cell type was as follows: B16/F10 – 1 × 10□ cells; MC-38 – 3 × 10□ cells; Panc02 – 3 × 10□ cells. For the bacterial experiment, mice were injected with 1 × 10□ B16/F10 cells without Matrigel. Once tumors were established (approximately 100 mm^3), tumor volume was measured every three days using digital calipers and calculated as: **volume = length × width² × 0.5**, where the width was the smaller of the two measurements. Treatment with diABZI and/or bile acids began when tumors reached ~250 mm^3 (Day 8) and was administered via intratumoral injection every three days. The doses per injection were as follows: CA or DCA – 2.5 mg/kg; diABZI – 50 µg/kg. Mice were euthanized when the tumor volume exceeded 2000 mm^3. For the survival assay, mice were considered dead when their tumor volume exceeded 2000 mm^3.

Cell isolation and flow cytometry analysis

Tumors, spleens, and tumor-draining lymph nodes (tdLNs) were dissected from mice. For tumor processing, excess stromal tissue was removed, and the tumor was placed in RPMI containing 1.5 U/mL Liberase TM (Roche, 5401119001), 0.2 mg/mL DNase I (Worthington Biochemical, LS002006), and ceramic spheres (6.35 mm, MP Biomedicals, 116540424-CF). The tissue was incubated at 37 °C with gentle shaking for 30 minutes, followed by passage through a 70 µm filter. For spleen processing, the spleen was transferred to a strainer, mashed using the end of a syringe, washed with RPMI, and centrifuged. Tumor and spleen samples were resuspended in 1 mL of red blood cell lysis buffer (Thermo Fisher, 00-4333-57) for 1–2 minutes at room temperature. For lymph nodes, tissues were directly mashed using the end of a 3 mL syringe and collected in 1 mL RPMI. Tumor, spleen, and tdLN cell suspensions were passed through 100 µm, 44% open area nylon mesh and transferred to 96-well plates.

Cells were washed and stained with 1:1000 Zombie Yellow viability dye (BioLegend, 423103) for 20 minutes at room temperature in the dark. After two washes, samples were incubated with 20 µL of staining buffer containing 0.5 µL TruStain FcX anti-mouse CD16/32 blocking agent (BioLegend, 101319) for 30 minutes at room temperature. Cells were then stained for 30 minutes on ice in the dark with the following antibodies: anti-CD4 (BUV496, GK1.5, BD Biosciences 612953), anti-CD44 (PerCP-Cy5.5, IM7, BioLegend 103031), anti-Sca-1 (BUV395, D7, BD Biosciences 563990), anti-CD69 (PE, H1.2F3, BioLegend, 104507) and anti-PD-1 (BV711, CD279, BD Biosciences 135231). Following staining, cells were washed twice, fixed, and permeabilized using the FoxP3/Transcription Factor Staining Buffer Set (Thermo Fisher, 00-5523-00) overnight at 4 °C. After three washes with permeabilization buffer, cells were incubated with 20 µL of permeabilization buffer containing 10% rat serum (Thermo Fisher, 24-5555-94) for 20 minutes on ice. Subsequently, cells were stained for 20 minutes on ice with the following antibodies: anti-CD45 (APC-Fire 750, 30-F11, BioLegend 103153), anti-CD3 (BV785, 17A2, BioLegend 100232), anti-NK1.1 (BV480, PK136, BD Biosciences 746265) anti-CD8 (PE-Cy-7, 53-6.7, BioLegend 100721), anti-FoxP3 (AF532, FJK-16s, Thermo Fisher 58-5773-80), anti-Granzyme B (PE-CF594, GB11, BD Biosciences 562462) and anti-Ki67 (FITC, SolA15, LifeTech 11-5698-82). Samples were analyzed using Cytek Aurora spectral flow cytometer, and data were analyzed using FlowJo Version 10.9.0.

Statistics:

Statistical analyses were conducted using GraphPad Prism 8.0. Briefly, pairwise comparisons were performed by using unpaired two-sided *t*-tests or two-sided Mann–Whitney tests. For comparisons of multiple groups with one variable, one-way analysis of variance (ANOVA) followed by multiple comparisons testing was used. For comparisons of multiple groups with

two variables, two-way ANOVA followed by multiple comparisons testing was used. Adjusted *P* values are provided for multiple comparisons. Specific statistical tests are identified in the corresponding figure legends. Comparisons with $P > 0.05$ were not considered significant.

Data Availability:

The data that support the findings in this work are available within the paper and Supplementary Information. All raw proteomics data files have been deposited to the PRIDE repository and available under the accession PXD056524. The atomic models and cryo-EM density maps generated in this study have been deposited to the PDB and EMDB with accession codes 9N7F and EMD-49094 respectively.

Additional Reference:

67. W. B. Jin *et al.*, Genetic manipulation of gut microbes enables single-gene interrogation in a complex microbiome. *Cell* **185**, 547-562.e522 (2022).
68. J. Tang *et al.*, Synthesis of portimines reveals the basis of their anti-cancer activity. *Nature* **622**, 507-513 (2023).
69. A. Punjani, J. L. Rubinstein, D. J. Fleet, M. A. Brubaker, cryoSPARC: algorithms for rapid unsupervised cryo-EM structure determination. *Nature Methods* **14**, 290-296 (2017).
70. A. Punjani, H. Zhang, D. J. Fleet, Non-uniform refinement: adaptive regularization improves single-particle cryo-EM reconstruction. *Nature Methods* **17**, 1214-1221 (2020).
71. T. D. Goddard *et al.*, UCSF ChimeraX: Meeting modern challenges in visualization and analysis. *Protein Science* **27**, 14-25 (2017).

72. P. Emsley, K. Cowtan, Coot: model-building tools for molecular graphics. *Acta Crystallographica Section D* **60**, 2126-2132 (2004).

73. P. Emsley, B. Lohkamp, W. G. Scott, K. Cowtan, Features and development of Coot. *Acta Crystallographica Section D* **66**, 486-501 (2010).

74. P. D. Adams *et al*., PHENIX: a comprehensive Python-based system for macromolecular structure solution. *Acta Crystallographica Section D* **66**, 213-221 (2010).

75. J. M. Word, S. C. Lovell, J. S. Richardson, D. C. Richardson, Asparagine and glutamine: using hydrogen atom contacts in the choice of side-chain amide orientation11Edited by J. Thornton. *Journal of Molecular Biology* **285**, 1735-1747 (1999).

Acknowledgments: We thank the Scripps Research Flow Cytometry and Imaging Cores for technical support.

Funding: This work was supported by National Institutes of Health (NIH) grants 1R01AI182439-01A1 to HCH, CGP, AW, LLL and GM069832 to S.F.

Author contributions: X.Y., X.Z., H.C.H conceived the study. X.Y., X.Z., W.L., A.G., A.H., A.T., C.W., Y.-Z.H., A.S., S.D. and X.Z. designed and performed methodology, investigation and visualization. H.C.H., C.G.P., A.W. and L.L.L. acquired funding. H.C.H. administered the project. Supervision was provided by H.C.H., C.G.P., A.W., L.L.L. and S.F. X.Y., X.Z. and H.C.H. wrote the original draft, and all authors contributed to review and editing of the manuscript.

Competing interests: LLL has filed and issued patents associated with synthetic STING agonists. All other authors declare that they have no competing interests.

Additional information:

Supplementary Information is available for this paper.

Correspondence and requests for materials should be addressed to Howard C. Hang.

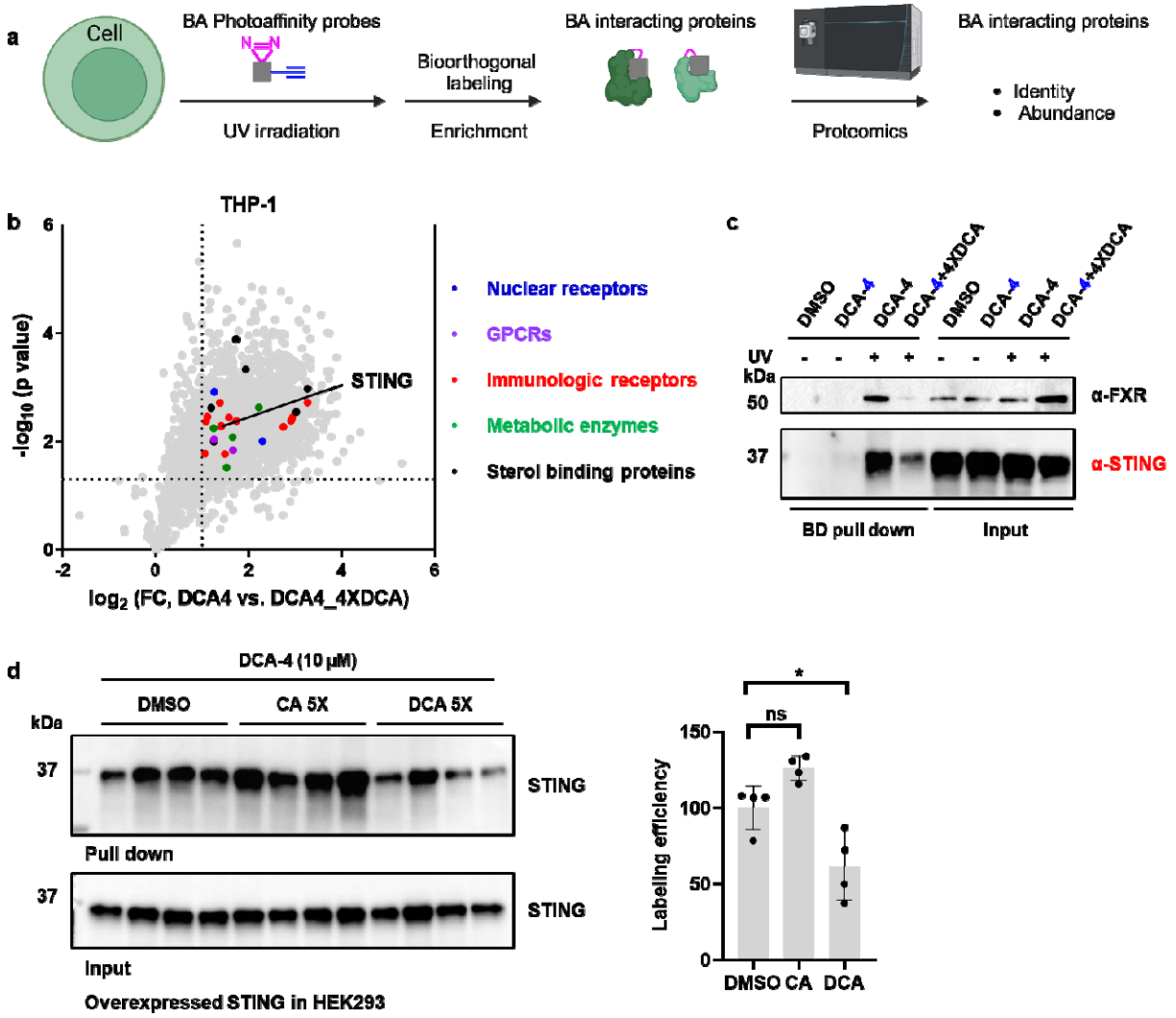

Extended Data Fig. 1 Chemoproteomic profiling of DCA-interacting proteins. (a) Chemoproteomics reveal the binding proteins of bile acid photoaffinity probes. (b) DCA4-enriched proteins are competed off by excess of DCA in THP-1 cells. STING is one of proteins that are selectively enriched by DCA photoaffinity reporters. Other DCA-enriched proteins are highlighted by different colors. (c) Validation of DCA-FXR/STING interaction in HT-29 by reverse western blot. HT-29 cells were treated with bile acid photoaffinity reporters with or without excess of DCA for 0.5□h, followed by 365-nm light irradiation. The labeled proteins were reacted with az-biotin and enriched with streptavidin beads ('pulldown'). Equal loading was validated by immunoblotting of input samples before enrichment ('input') (d) Validation of DCA-STING interaction in HEK293T by reverse western blot. HEK293T transfected with pMSCV-hygro-STING were treated with DCA-4 in presence or absence of 5X CA and 5X DCA for 0.5□h,

followed by 365-nm light irradiation. The labeled proteins were reacted with az-biotin and enriched with streptavidin beads (‘pulldown’). Equal loading was validated by immunoblotting of input samples before enrichment (‘input’) (n = 4 biologically independent samples). A one-way ANOVA followed by Tukey’s multiple comparisons test was used to calculate the adjusted P values. *P < 0.05, **P < 0.01, ***P < 0.001, ****P < 0.0001; ns, not significant.

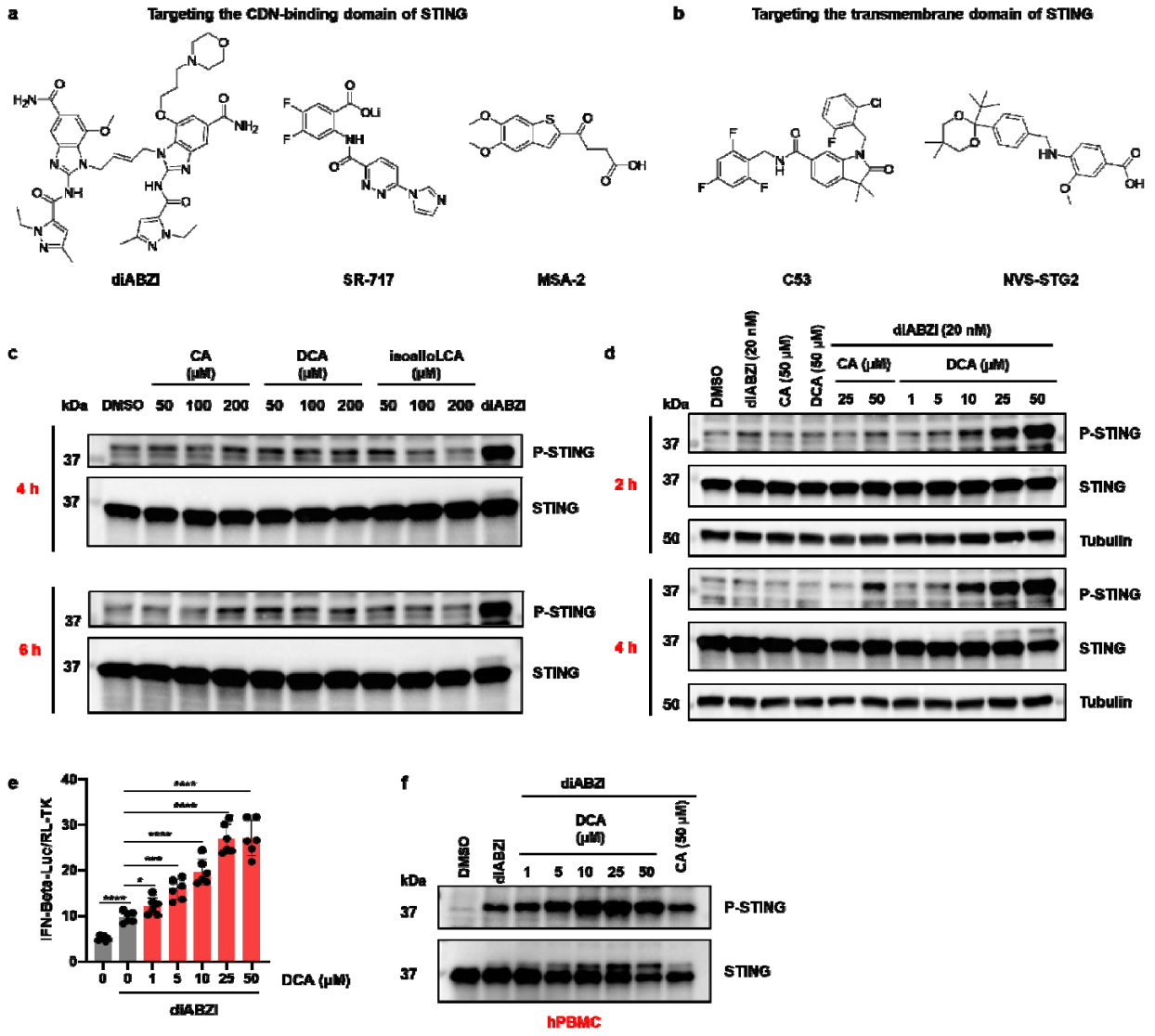

Extended Data Fig. 2 Bile acids synergize with STING agonists to promote STING activation ex vivo. (a) Chemical structure of STING agonists targeting CDNs binding domain. (b) Chemical structure of STING agonists targeting SING transmembrane domain. (c) Western blot analysis of cell lysates from THP-1 cells treated with diABZI (100 nM) and different concentrations of bile acids (50, 100, 200 μM) alone for 4 or 6 hours. (d) Western blot analysis of cell lysates from THP-1 cells treated with diABZI (20 nM), CA (25, 50 μM) and DCA (1, 5, 10, 25, 50 μM) alone or together for 2 or 4 hours. (e) HEK293T transfected with pMSCV-hygro-STING, IFN-Beta_pGL3 and pRL-TK control plasmid were treated with diABZI (20 nM) in presence or absence of different dose of DCA (*n*

= 6 biologically independent samples). Data were analyzed by unpaired two-sided t-test. (f) Western blot analysis of cell lysates from Human PBMCs treated with diABZI (200 nM) in presence or absence of DCA and CA for 2 hours.

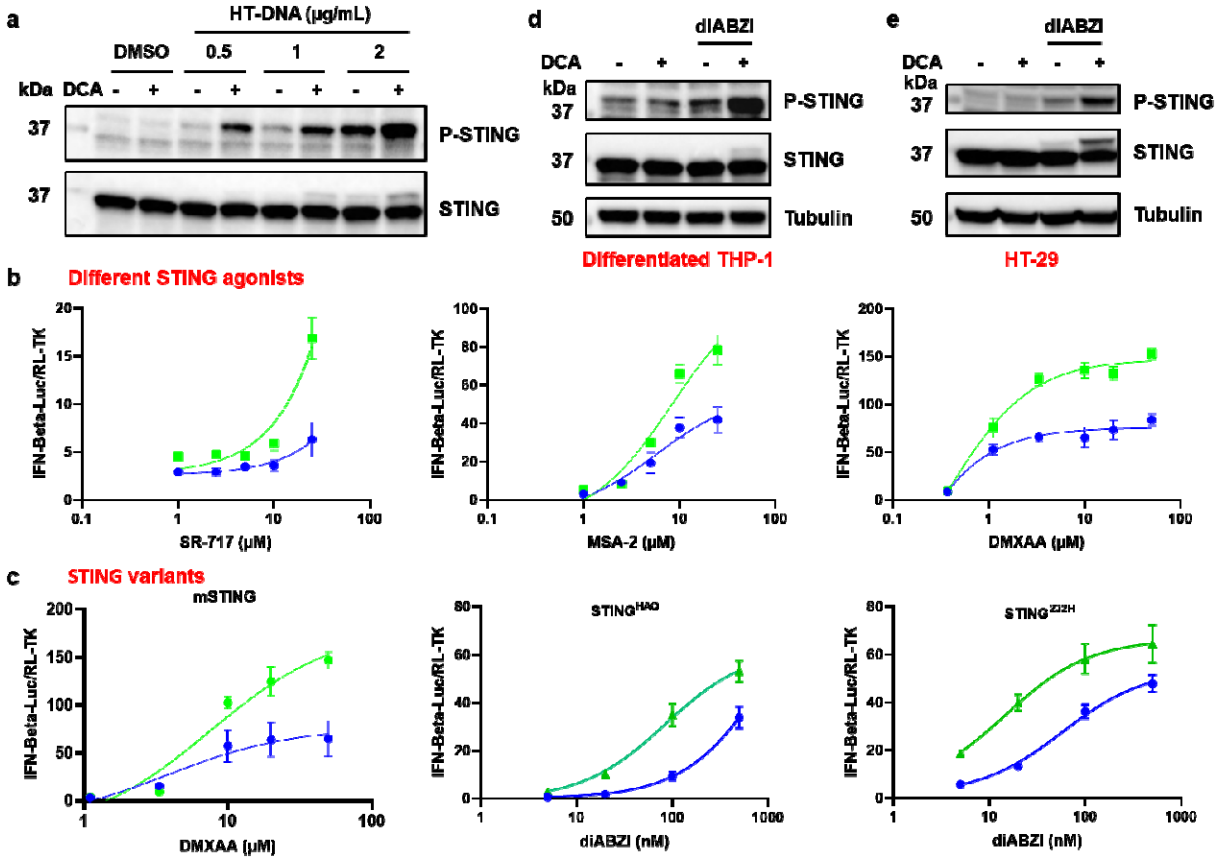

Extended Data Fig. 3 The generality of DCA activity on STING activation. (a) Western blot analysis of cell lysates from differentiated THP-1 cells (pretreat the cells with 100 nM of PMA for 24 h) treated with different concentrations of HT-DNA (0.5, 1, 2 μg/mL, HT-DNA was transfected by Lipo2000 (1 μg/μL)) in presence or absence of DCA (50 μM). (b) HEK293T cells transfected with pMSCV-hygro-STING, IFN-Beta_pGL3 (a luciferase reporter plasmid under control of the IFN-β promoter) and pRL-TK control plasmid were treated with different STING agonists (SR-717, MSA-2 and DMXAA) in presence or absence of DCA (50 μM). For DMXAA, pMSCV-hygro-STING(S162A, G230I, Q266I) was used (n = 3 biologically independent samples). (c) HEK293T transfected with different STING variants (pMSCV-hygro-murineSTING, pMSCV-hygro-STING HAQ and pMSCV-hygro-STING R232H), IFN-Beta_pGL3 (a luciferase reporter plasmid under control of the IFN-β promoter) and pRL-TK control plasmid were treated with STING agonist (DMAXX or diABZI) in presence or absence of DCA (50 μM) (For mSTING, n = 3, for $STING^{HAQ}$, n = 5, for $STING^{232H}$, n = 4, biologically independent samples). (d) Western blot analysis of cell lysates from differentiated THP-1 cells (pretreat the cells with 100 nM of

PMA for 24 h) treated with diABZI (50 nM) in presence or absence of DCA (50 µM). (e) Western blot analysis of cell lysates from HT-29 cells treated with diABZI (50 nM) in presence or absence of DCA (50 µM).

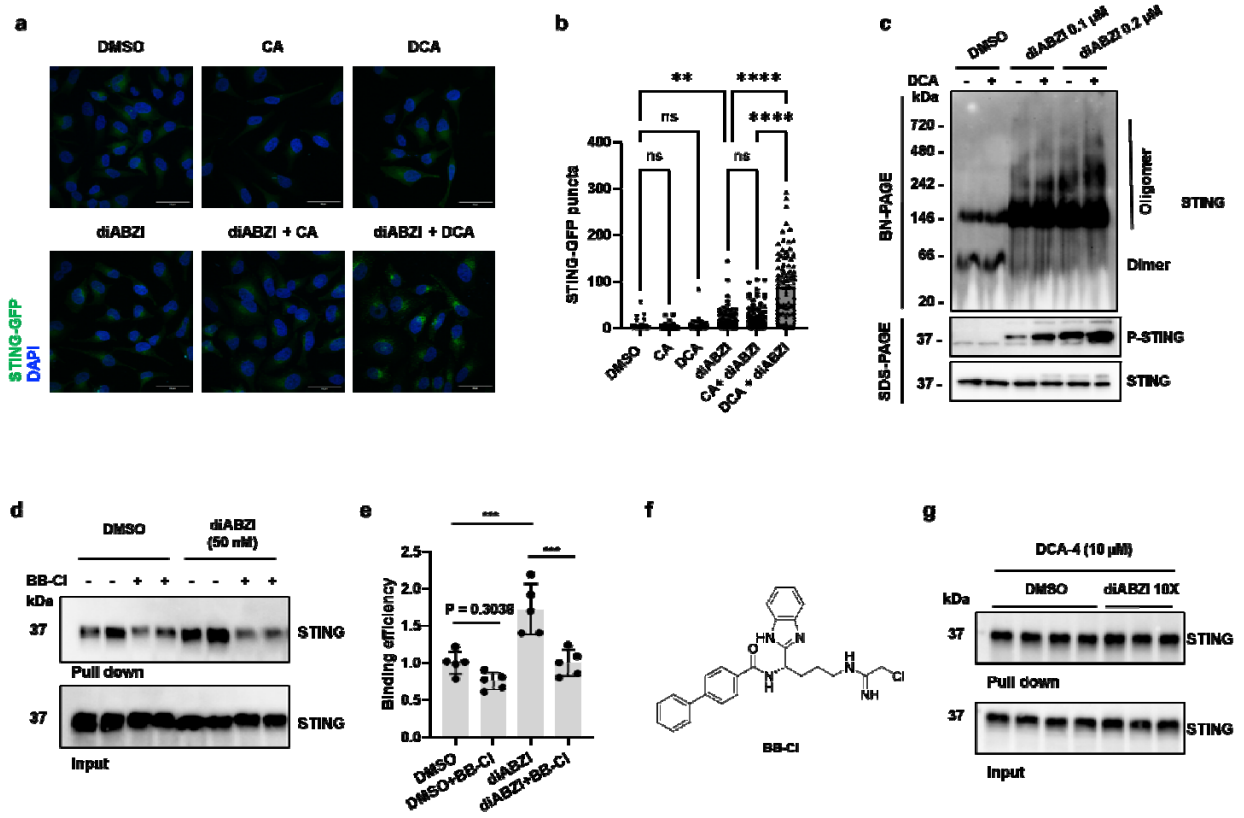

Extended Data Fig. 4 DCA promotes diABZI-induced STING oligomerization. (a) Representative images of HeLa cells stably expressing STING-GFP. Cells were treated with CA (50 μM) or DCA (50 μM), in the presence or absence of diABZI (50 nM), using equal volume of DMSO as a control. Localization of STING-GFP in cells was monitored by the fluorescence signal of GFP puncta. Nuclei were counter-stained with DAPI. The experiments were repeated three times. The images are representative images from these experiments. (b) Quantification of intracellular STING puncta. The bar graph shows the amount of STING puncta per cell from each treatment group. Data represent mean ± SD and were analyzed by the one-way ANOVA with Šídák's multiple comparisons test. *P < 0.05, **P < 0.01, ***P < 0.001, ****P < 0.0001; ns, not significant. Scale bar, 50 μm. (c) STING oligomerization induced by DCA, diABZI or both. THP1-Dual cells were stimulated with DCA (50 μM) in presence or absence of diABZI (100, 200 nM) for 2 hours. STING oligomerization was analyzed by Blue native PAGE (BN-PAGE), and the indicated proteins were detected by immunoblotting. (d) THP-1 cells were pretreated with diABZI (50 nM) in presence or absence of BB-Cl (10 μM) for 1 hour. Cells were then treated with DCA-4 (25 μM) for another 0.5 hour, followed by 365-nm light irradiation. The labeled proteins in cell lysis were reacted with az-biotin and enriched with

streptavidin beads (‘pulldown’). Equal loading was validated by immunoblotting of input samples before enrichment (‘input’). (e) Quantification of DCA-4 STING binding efficiency in C by grayscale analysis (pull down/input) (*n* = 3 biologically independent samples). A one-way ANOVA followed by Tukey’s multiple comparisons test was used to calculate the adjusted P values. (f) Chemical structure of an inhibitor of STING activation, BB-Cl. (c) Validation of DCA-STING interaction in HEK293T overexpressed STING n presence or absence of excess of diABZI by reverse western blot. HEK293T transfected with pMSCV-hygro-STING were treated with DCA-4 in presence or absence 10X diABZI for 0.5 h at 37 ºC, followed by 365-nm light irradiation. The labeled proteins were reacted with az-biotin and enriched with streptavidin beads (‘pulldown’). Equal loading was validated by immunoblotting of input samples before enrichment (‘input’). *P < 0.05, **P < 0.01, ***P < 0.001, ****P < 0.0001; ns, not significant.

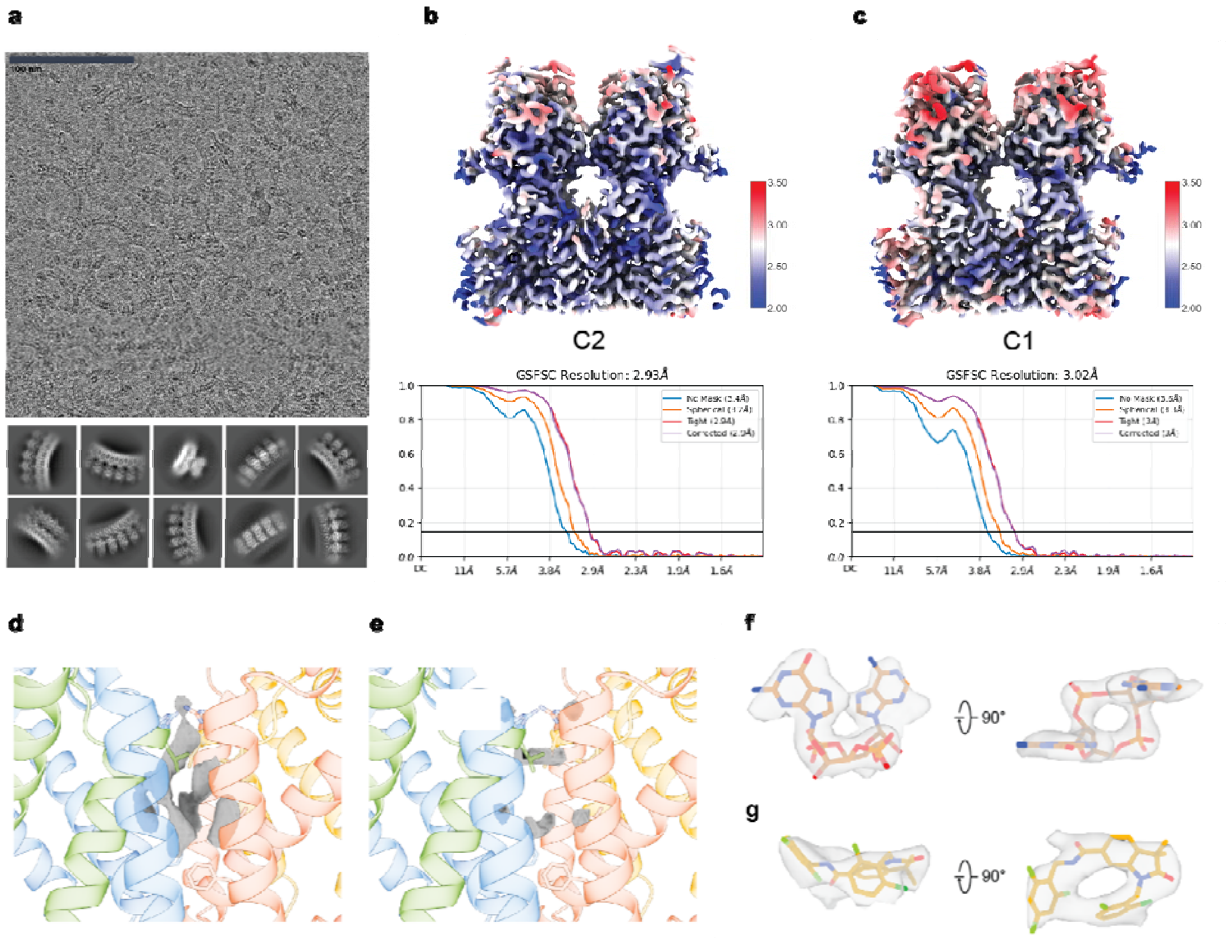

Extended Data Fig. 5 Cryo-EM analysis of STING binding with different agonists. (a) Motion corrected micrograph and 2D class averages of high-order oligomers of human STING. (b,c) 3D reconstruction of the STING tetramer complexed with ligands (cGAMP and C53), and gold-standard FSC curve of the final 3D reconstruction. (d,e) High-resolution cryo-EM map of the two STING dimer with highlight of dimer-dimer interface molecular density. (d: STING, cGAMP, C53 and DCA (C1 symmetry, this study); e: STING, cGAMP, C53 (PDB ID: 7SII)) (f) CryoEM density for cGAMP. (g) CryoEM density for C53.

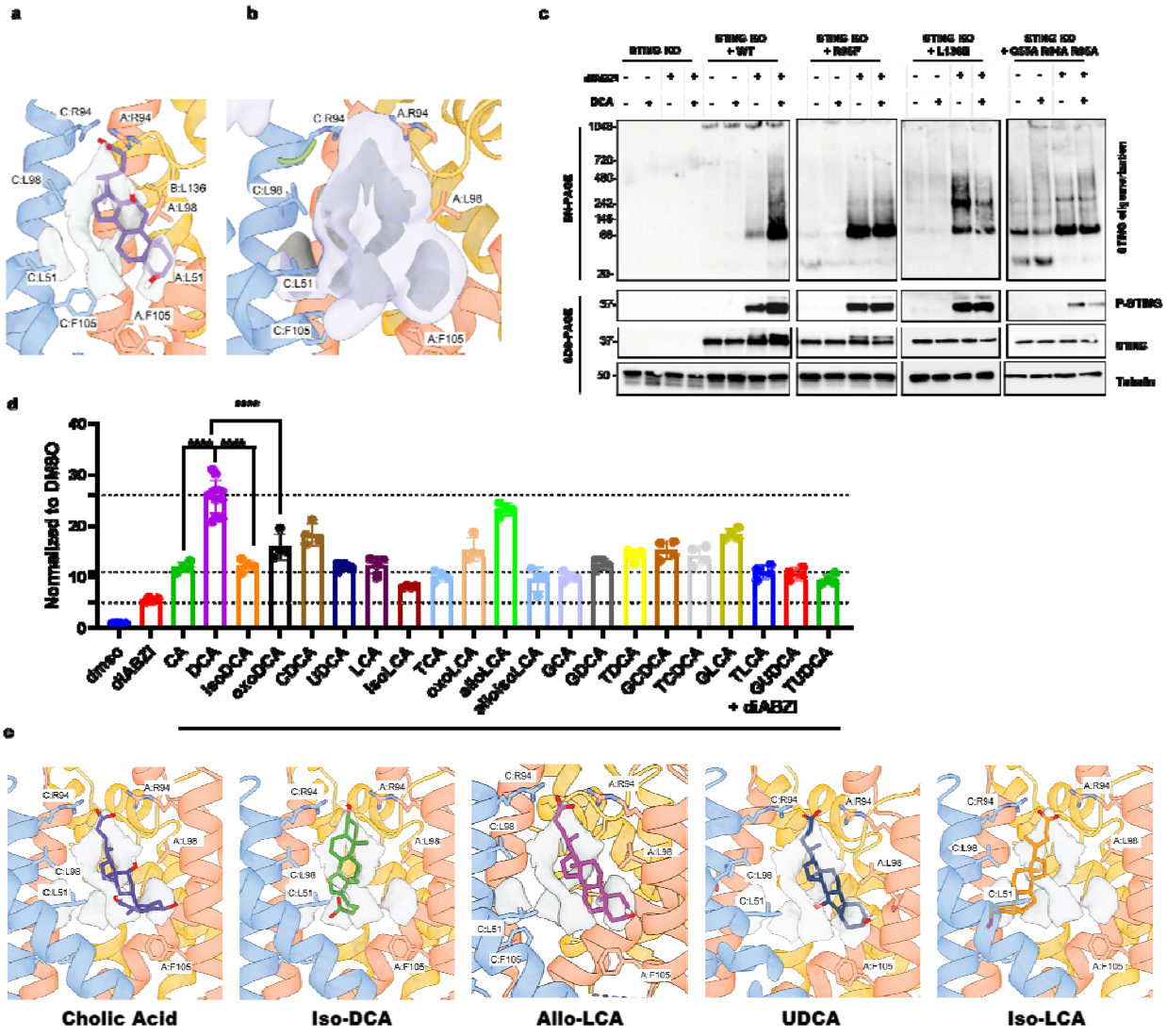

Extended Data Fig. 6 Reponses of hSTING to different bile acids, with key binding pocket mutations. (a) Docked model of DCA in STING tetramer. Docking guided by C2-symmetric density, shown in gray. (b) Illustration of docking density cloud (outer violet surface), representing Boltzmann-weighted map of ligand states sampled during docking simulation. All experimental density lobes on one side of the binding pocket were sampled during the simulation, but less so on the opposite side of the pocket. (c) STING oligomerization induced by DCA, diABZI or both. THP1-Dual STING KO cells (STING-WT, STING R95F, STING L136E, STING Q55A+R94A+R95A stable expression cell lines) were stimulated with DCA in presence or absence of diABZI for 2 hours. STING oligomerization was analyzed by Blue native PAGE (BN-PAGE), and the indicated proteins were detected by immunoblotting. (d) HEK293T transfected with pMSCV-hygro-STING, IFN-Beta_pGL3 (a luciferase

reporter plasmid under control of the IFN-β promoter) and pRL-TK control plasmid were treated with diABZI (20 nM) in presence or absence of different conjugated and free bile acids (50 μM) (For DCA, $n = 12$, and others $n = 4$, biologically independent samples). Data were analyzed by unpaired two-sided t-test. (e) Docked models of Cholic Acid, Iso-DCA, UDCA, Iso-LCA and alloLCA in STING tetramer. Dockings guided by C2-symmetric density for DCA, shown in gray. Cholic acid, UDCA and alloLCA adopt binding poses like that predicted for DCA. However, alloLCA lacks an additional hydroxyl group that may stabilize the STING tetramer more like DCA. Iso-DCA, meanwhile, is the only ligand to orient the carboxylate down into the bottom of the pocket, with a hydroxyl hydrogen bonding with R94 of the C monomer. Iso-LCA also adopts a different binding mode from cholic acid. While Iso-LCA does place the carboxylate in a salt bridge with R94 of the A and C monomers, the rest of the molecule is oriented with interactions with the C monomer. All static poses for all of the tested bile acids were consistent across simulation runs. *P < 0.05, **P < 0.01, ***P < 0.001, ****P < 0.0001.

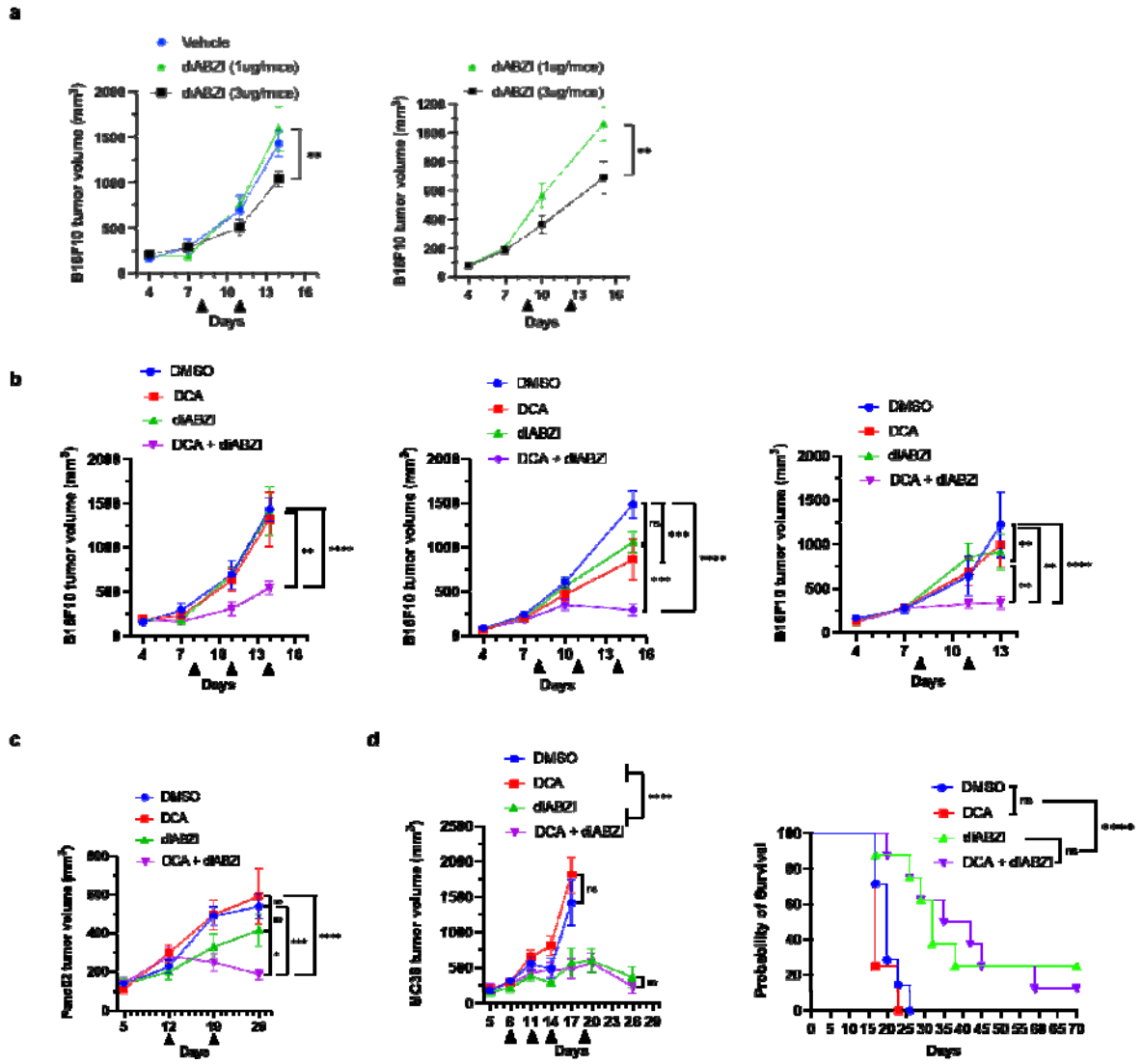

Extended Data Fig. 7. The effect of DCA on STING-mediated anti-tumor activity in different tumor models. (a) Comparison of B16-F10 tumor growth following it. injection of two different concentrations of diABZI. (b) All the other repeats for B16-F10 melanoma tumor experiments. (c) Panc02 tumor growth in mice treated i.t. with vehicle (DMSO), DCA, diABZI, or the combination. (d) MC38 tumor growth and survival in SPF mice that were IT injected with vehicle (DMSO), bile acids DCA, diABZI or the combination (DCA+ diABZI). Arrowhead indicates the day for it. injection. n = 8 mice per group. Data represent mean ± SEM and were analyzed using a mixed effects model with Tukey's multiple comparisons post hoc test. **P < 0.01, ***P < 0.001, ****P < 0.0001; ns, not significant.

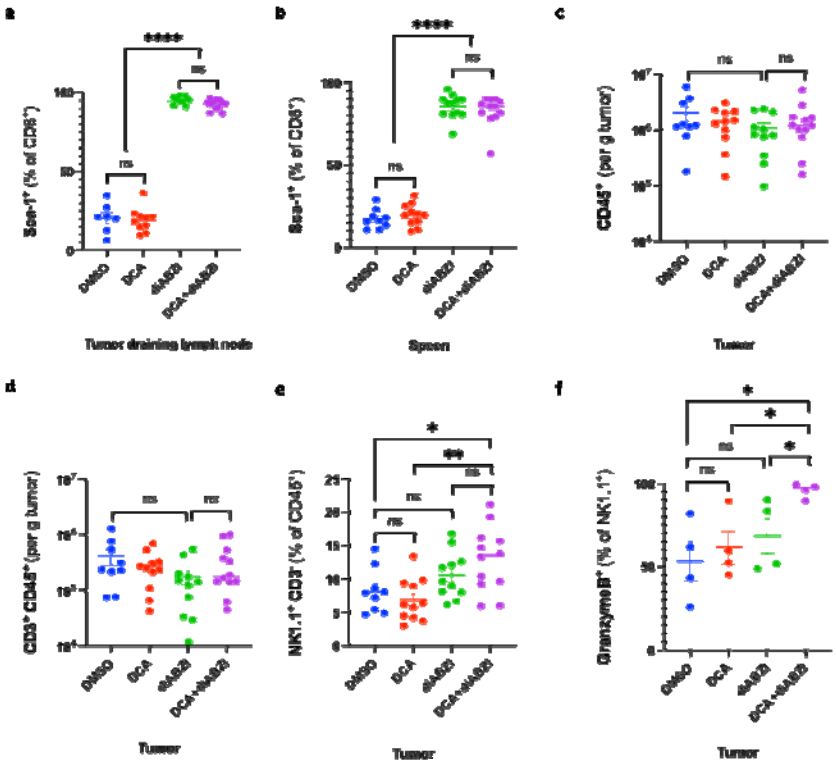

Extended Data Fig. 8. DCA synergizes STING activation to promote antitumor immunity *in vivo*. (a, b), Percentage of Sca-1^{+} cells among CD8□ T cells in the tdLN (a) and spleen (b). (c) Quantification of tumor infiltrating CD45^{+} cells. (d) Quantification of tumor infiltrating CD3^{+} CD45^{+} cells. (e) Quantification of tumor infiltrating NK1.1^{+} CD3^{+} cells. (f) Quantification of tumor infiltrating Granzyme B^{+} NK1.1^{+} cells. Data for a-e were pooled from two independent experiments. n = 9-12 per group. Data for f represents a single representative experiment, with n = 4 per group. All the data represent mean ± SEM and were analyzed by the unpaired t test. *P < 0.05, **P < 0.01, ****P < 0.0001; ns, not significant.

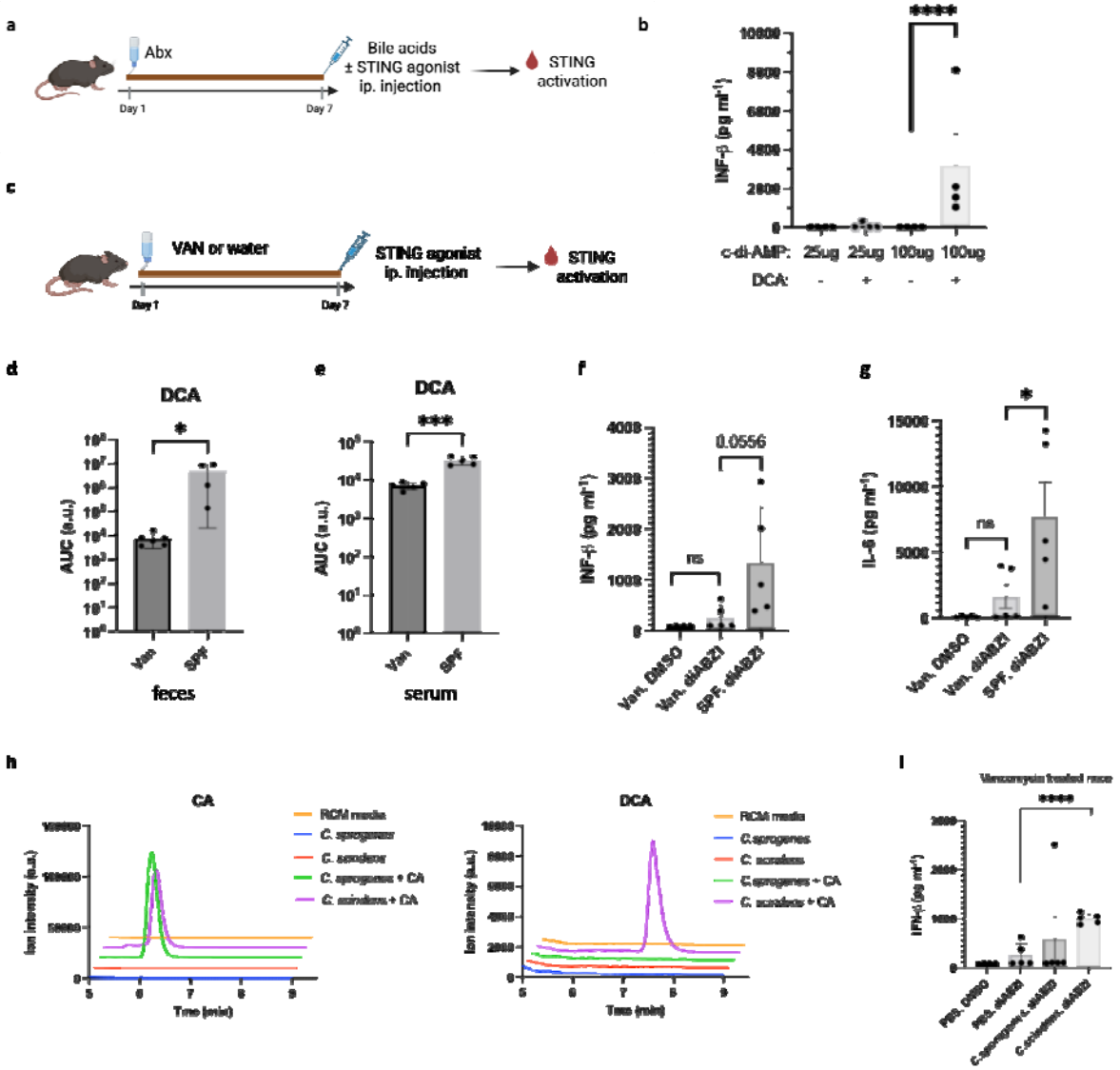

Extended Data Fig. 9. DCA and DCA-producing bacteria enhance STING-mediated type I interferon signaling *in vivo*. (a, b), Mice were treated with Abx for 1 week, then received i.p. injection of two different concentration of c-di-AMP with or without DCA. Four hours post-injection, serum IFN-β levels were measured by ELISA. *n* = 4 mice per group. (c-g) Mice were treated with or without vancomycin for 1 week. On Day 7, fecal (d) and serum (e) DCA levels were measured by LC-MS. Four hours following diABZI injection, serum IFN-β (f) and IL-6 (g) were quantified by ELISA. *n* = 5 mice per group. Data are presented as mean ± SEM and analyzed by unpaired two-tailed t-test. (h) Extracted ion chromatograms (EIC) showing CA (m/z = 407.2) and DCA (m/z = 391.2) from bacterial cultures grown in RCM media with or without added CA. (i) Mice were treated with vancomycin for 7 days. On Day 7, vancomycin was replaced with water, and mice were orally

gavaged daily with *C. sporogenes* or *C. scindens* for 3 consecutive days. On Day 10, mice were i.p. injected with diABZI. Four hours later, serum was collected for IFN-β quantification by ELISA. n = 5 mice per group. Data are presented as mean ± SEM and analyzed by unpaired two-tailed t-test. *P < 0.05; ***P < 0.001; ****P < 0.0001; ns, not significant.

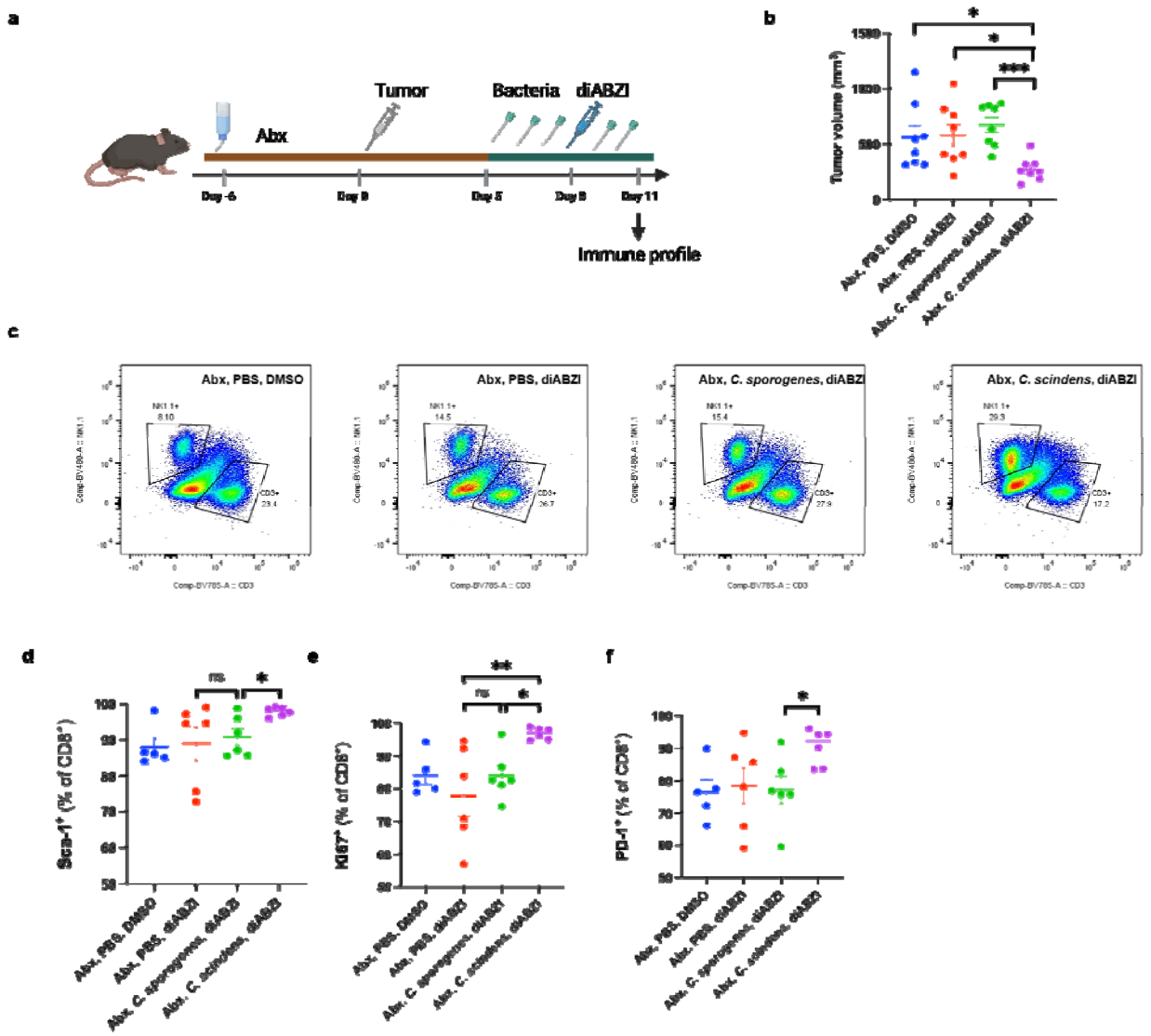

Extended Data Fig. 10. Analysis of specific microbiota species on STING agonist-mediated antitumor immunity *in vivo*. (a) Mice were treated with Abx for 10 days. On Day 5 post-tumor implantation, Abx was stopped, and mice were started daily oral gavage with PBS, *C. sporogenes*, or *C. scindens*. A single dose of diABZI were administered on Day 8, and tumors were collected for flow cytometry on day11. (b) Tumor size at the day of

collection (Day11). *n* = 8 mice per group. Data represent mean ± SEM and were analyzed using a mixed effects model with Tukey's multiple comparisons post hoc test. (c) Representative plots of single cell suspensions harvested from B16F10 tumors corresponding to Fig. 5j-l. Graphs depict $NK1.1^{+}$ $CD3^{-}$ and $NK1.1^{-}$ $CD3^{+}$ tumor infiltrating cells. (d-f) Quantification of tumor-infiltrating CD8 T cells expressing Sca-1 (d), Ki67 (e), or PD-1 (f). n = 5–6 mice per group, represent mean ± SEM and were analyzed using unpaired two-tailed *t*-test. *P < 0.05, **P < 0.01, ***P < 0.001; ns, not significant.